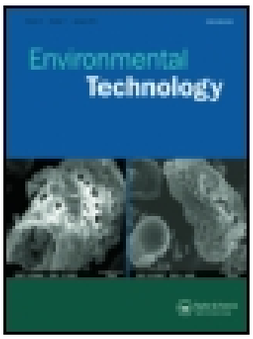

Environmental Technology

ISSN: (Print) (Online) Journal homepage: https://www.tandfonline.com/loi/tent20

Highly efficient capture of mercury from complex water matrices by AlZn alloy reduction-amalgamation and *in situ* layered double hydroxide

Yetian Fang, Fangyuan Li, Jingbo Chao, Yang Tang, Frederic Coulon, Patrycja Krasucka, Patryk Oleszczuk, Qing Hu & Xiao Jin Yang

To cite this article: Yetian Fang, Fangyuan Li, Jingbo Chao, Yang Tang, Frederic Coulon, Patrycja Krasucka, Patryk Oleszczuk, Qing Hu & Xiao Jin Yang (2023): Highly efficient capture of mercury from complex water matrices by AlZn alloy reduction-amalgamation and *in situ* layered double hydroxide, Environmental Technology, DOI: 10.1080/09593330.2023.2180437

To link to this article: https://doi.org/10.1080/09593330.2023.2180437

Environmental Technology, Available online 13 February 2023
DOI: 10.1080/09593330.2023.2180437

Publisher: Taylor & Francis & Informa UK Limited, trading as Taylor & Francis Group
Journal: *Environmental Technology*
DOI: 10.1080/09593330.2023.2180437

Highly efficient capture of mercury from complex water matrices by AlZn alloy reduction-amalgamation and *in situ* layered double hydroxide

Yetian Fang [a], Fangyuan Li [a], Jingbo Chao [b], Yang Tang [c], Frederic Coulon [d], Patrycja Krasucka [e], Patryk Oleszczuk [e], Qing Hu [f, g], Xiao Jin Yang [a] *

[a] State Key Laboratory of Chemical Resource Engineering, Beijing University of Chemical Technology, Beijing 100029, China.
[b] National Institute of Metrology, Beijing 100029, China.
[c] National Fundamental Research Laboratory of New Hazardous Chemicals Assessment and Accident Analysis, Beijing University of Chemical Technology, Beijing, 100029, China
[d] School of Water, Energy and Environment, Cranfield University, Cranfield MK43 0AL, UK.
[e] Faculty of Chemistry, Department of Radiochemistry and Environmental Chemistry, Maria Curie-Sklodowska University, 3 M. Curie-Sklodowska Sq., 20-031 Lublin, Poland.
[f] Southern University of Science and Technology, Shenzhen, Guangdong 518055, China.
[g] Beijing Huanding Environmental Big Data Institute, No. 1 Wangzhuang Road, Beijing 100083, China.
*Corresponding Author: yangxj@mail.buct.edu.cn (X. J. Y.).
ORCID: Xiao Jin Yang: 0000-0003-4113-9298

Abstract

Mercury pollution is a critical, worldwide problem and the efficient, cost-effective removal of mercury from complex, contaminated water matrices in a wide pH range from strongly acidic to alkaline has been a challenge. Here, AlZn and AlFe alloys are investigated and a new process of synergistic reduction-amalgamation and *in situ* layered double hydroxide (SRA-*i*LDH) for highly efficient capture of aqueous Hg(Ⅱ) is developed using AlZn alloys. The parameters include the pH values of 1-12, the Hg(II) concentrations of 10-1000 mg L^{-1}, and the alloy's Zn concentrations of 20, 50 and 70% and Fe concentrations of 10, 20 and 50%. The initial rate of Hg(Ⅱ) uptake by AlZn alloys decreases with increasing Zn concentration while the overall rate is not affected. Specifically, AlZn50 alloy removes >99.5% Hg(Ⅱ) from 10 mg L^{-1} solutions at pH 1-12 in 5 min at a rate constant of 0.055 g mg^{-1} min^{-1} and achieves a capacity of 5000 mg g^{-1}, being the highest value reported so far. The super-performance of AlZn alloy is attributed to multiple functions of chemical reduction, dual amalgamation, *in situ* LDH's surface complexation and adsorption, isomorphous substitution and intercalation. This study provides a simple and highly efficient approach for removing Hg(Ⅱ) from complex water matrices.

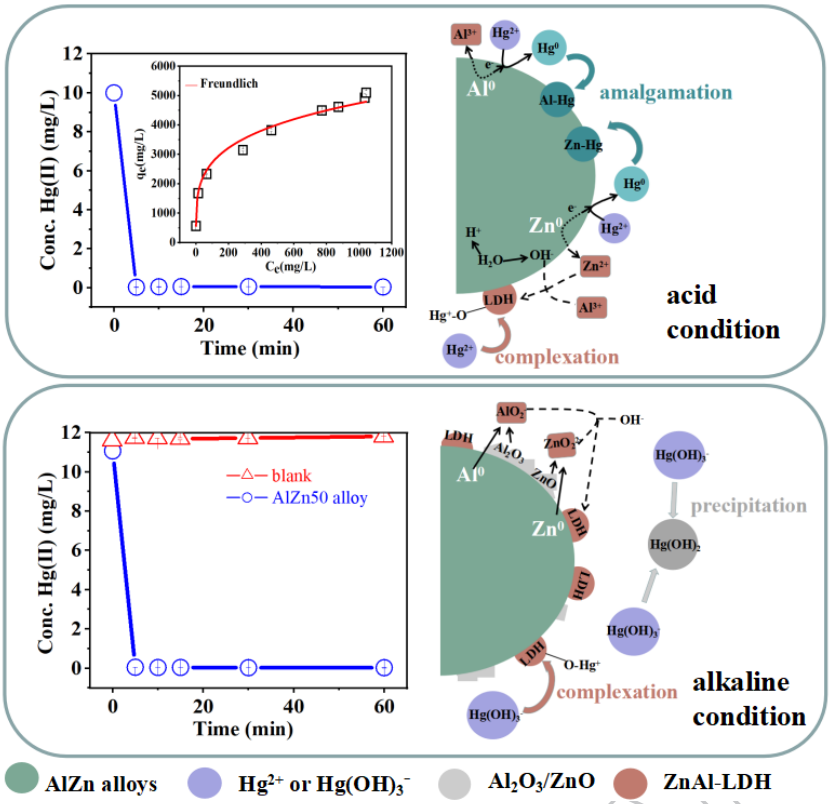

Keywords: Mercury; Wastewater; Aluminum-zinc alloy; Reductive amalgamation; *in situ* layered doubled hydroxide

1. Introduction

Mercury pollution is a worldwide problem [1-3] and the efficient remediation of inorganic mercury contaminated water[3], particularly in strongly acidic conditions has been long a challenge [4, 5]. Many technologies including membrane filtration [6], adsorption [7] and reductive amalgamation [8, 9] are applied to remove inorganic mercury ions Hg(Ⅱ) from aqueous environments. Adsorption is simple and effective and the development of advanced adsorbent materials for Hg(Ⅱ) removal has been active both in traditional adsorbents and emerging nanomaterials such as layered double hydroxides (LDH) [10, 11], metal-organic framework (MOF) [12, 13] and covalent-organic framework (COF) [14]. In general, the adsorbents requires meticulous and in many cases, complicated molecular design and introducing functional groups and sulfur derivatives such as thiol and thioether. The adsorption capacity of Hg(Ⅱ) reached 510, 2100, 2560, 4400 mg g^{-1} by NiCo-LDH/MOF [15], PCuS [16], MoS_2 [17] and TPB-DMTP-COF-SH [18], respectively. Further improvement is difficult because of the limitations of sulfur content and utilization (e.g., buried chelation sites and low degree of functionalization). These complex materials were extremely sensitive to pH and the adsorption efficiency was significantly deteriorated in low pH ranges [15, 17, 19]. For instance, the maximum Hg(II) capture capacity of MIL88A-SH is only shown at pH 5-8 [20] and TPB-DMTP-COF-SH [18] was effective at pH >5.4. In addition, the extremely high cost prevents the large-scale environmental applications of MOF and COF-based materials [21, 22].

Zerovalent metals with low oxidation potentials (e.g., Al, Fe, Mg and Zn) are efficient to remove high oxidation potential heavy metals including Hg(Ⅱ) via chemical reduction. Zerovalent iron (ZVI) suffers many problems including rapid passivation, particularly in pH 4.5 and above, secondary pollution and poor capacity (<10 mg g^{-1}) [23-25]. Zerovalent aluminum (ZVAl) was reported to avoid some restrictions of the ZVI technology for water remediation, but their applications are also limited, due primarily to the high-dense protective layer of alumina, which is required to be removed by pretreatment using chemicals and acids [26-28]. To overcome the shortcomings of ZVI and ZVAl, researchers investigated bimetals [9, 19, 29-31] (e.g., Fe-Al, Fe-Ni, Fe-Cu, In-Fe), which are generally prepared using wet chemical methods by chemically depositing a secondary metal catalyst. However, the uniform distribution of the secondary metal catalyst on the surface of the primary one is difficult to control and the exfoliation of the catalyst metal is inevitable during water treatment such that the performance is unpredictable and secondary contamination is a serious concern. AlFe, AlNi, AlCu and CuZn alloys [32-37] were reported to avoid the instability of bimetals for water remediation, but secondary contamination was still problematic apart from poor

capacities. To the best of our knowledge, efficient capture of Hg(II) from highly acidic water matrices free of secondary contamination has been a challenge [15-18].

Recently, we reported a new concept of MgAl alloy's *in situ* LDH for the removal of Cd, Cu, Cr, Ni and Zn and organic pollutants from contaminated, acidic water and found that the *in situ* LDH formation not only improved the removal performance significantly also eliminated the secondary contamination [38]. Herein, we consider that AlZn alloys could be a highly efficient material to capture aqueous Hg(Ⅱ) over a wide pH range from strongly acidic to alkaline while eliminating Al secondary contamination if ZnAl-LDH could be *in situ* generated, creating a new process of synergistic reduction-amalgamation-*in situ* layered double hydroxide (SRA-*i*LDH). To demonstrate this new concept, we investigated AlZn and AlFe alloys, Al, Fe and Zn metal powders to capture aqueous Hg(Ⅱ) from complex water matrices.

2. Materials and Methods

2.1 Chemicals and materials

Al, Fe and Zn metal powders (75-150 μm) were purchased from Tianjin Fuchen Chemical Reagent Factory (China). AlZn alloys (20, 50 and 70% Zn), AlFe alloys (10, 20 and 50% Fe) and AlSi10, AlCu15 were obtained from Hunan Changsha Tianjiu Co., Ltd. (China). The particle size of AlZn50 powders and AlCu15 were <10 μm (D50 = 9-11μm) and that of AlZn20, AlZn70, AlSi10 and AlFe alloys was <75 μm. Certified reference materials of mercury (GBW08617), aluminum (GBW(E) 080219), zinc (GBW(E) 080130) and mixed multi-elements solution (GBW(E) 081532-081535) were obtained from the National Institute of Metrology (China). $Hg(NO_3)_2{\cdot}H_2O$ (97.0%) was purchased from Dalian Xiangde Chemical Co., Ltd. (China). HNO_3 (69%), HCl (37%) and NaOH (99.7%) were purchased from Beijing Chemical Works (China). Mercury solutions (10-2000 mg L^{-1}) were prepared by dissolving $Hg(NO_3)_2{\cdot}H_2O$ in high-purity water and adjusted to a certain pH using dilute HCl and NaOH solutions. High-purity water (18 MΩ) was prepared using Millipore, USA.

2.2 Pretreatment of AlZn50 alloy

1 g of AlZn50 alloy was added to 100 mL of pH 1 HCl solution and subjected to magnetic stirring for 72 hours. The suspension was centrifuged, filtered, and dried in a vacuum drying oven at 80°C for 24 hours and the pretreated AlZn50 alloy was term as p-AlZn50.

2.3 Batch experiment

A mercury solution of 45 mL was added into a 100 mL glass bottle and loaded with 0.5 g adsorbent material (Al, Fe, Zn, AlZn alloys, AlFe alloys, p-AlZn50). The Hg(Ⅱ) concentration was 10 mg L^{-1} and solution pH was 2, unless otherwise specified. The solution was stirred at 300 rpm with a magnetic bar under ambient conditions. For kinetic studies, the volume of mercury solution and the mass of adsorbent material were doubled and an aliquot sample of 3 mL was taken at a certain interval for analysis of metal ions and pH measurement. The removal efficiency E (%) and removal capacity q_e (mg g^{-1}) of Hg(Ⅱ) are calculated by the following equations,

$$E(\%) = \frac{C_0 - C_e}{C_0} \times 100$$

$$q_e = \frac{(C_0 - C_e)}{m} \times V$$

where C_0 and Ce are the initial and equilibrium concentration of Hg(Ⅱ) (mg L^{-1}) in the solution, V is the volume of solution (L) and m is the amount of material (g) added. All experiments were performed in three independent samples.

2.4 Reuse of AlZn50 alloy

After the batch experiment, the solution was centrifuged at 5000 rpm and filtered. The precipitates were washed with high-purity water to neutral pH and freeze-dried for 24 h. Then, the material (0.5 g) was added to a 10 mg L^{-1} mercury solution of 45 mL for a second cycle of Hg capture. Five cycles were conducted.

2.5 Material characteriction and measurement of metal ion concentration

The surface morphology of the material and the compositional structure were analysed by scanning electron microscope (SEM) (JEOL, JSM-7001F, Japan) and X-ray diffraction (XRD) (Rigaku Corporation, Ultima IV, Japan). The elements and valence states contained in the materials were detected by X-ray Photoelectron Spectroscopy (XPS) (Shimadzu, Axis Supra, UK). The functional group structure in the material was characterized by infrared spectroscopy (FTIR) (BRUKER, TENSOR27, Germany). Al, Zn, Hg concentrations were detected by ICP-OES (Thermo, iCAP 7400DUO, U.S.A.). Desktop freeze dryer (Beijing Bo Yikang Experimental Instrument Co., Ltd., FD-1A-50, China).

3. Results and Discussion

3.1 Effect of Zn content of AlZn alloys

Aqueous Hg(Ⅱ) capture by AlZn alloys may involve chemical reduction, amalgamation adsorption and

coprecipitation of Hg(Ⅱ) hydroxide in accordance with chemical properties of Al and Zn metals. Fig. 1 shows the effect of Zn content of AlZn alloys on Hg(Ⅱ) capture, solution pH variation and leached concentration of Al and Zn ions. For comparison, zero-valent Al and Zn powders are included. Greater than 99.5% of 10 mg L^{-1} Hg(II) are removed in 3 min by AlZn20 and AlZn50 alloys at an initial pH 3 while the removal rates by Zn and AlZn70 are slower (92.3% and 73.3% in 3 min) and Hg removal by Al is negligible (**Fig. 1a**). The pH of the solution in the AlZn alloy system increases rapidly from 3 to 6 in 3 min and then stabilizes; the pH of the solution remains almost unchanged from initial pH value in the Al system while it increases to 7.3 in 60 min in the AlZn50 system (**Fig. 1b**).

Apparently, Al is significantly activated for Hg(Ⅱ) capture by alloying with Zn. The concentration of Al ions leached is extremely low at 0.03-1.0 mg L^{-1} in the cases of Al, AlZn20 and AlZn70 alloy (**Fig. 1c**) while it increases slowly to 10 mg L^{-1} in 30 min and then rapidly to 93 mg L^{-1} in 60 min in the case of AlZn50 alloy (**Fig. 1c**). Interestingly, Zn ion concentration is lifted to 38-45 mg L^{-1} in 3 min in this case while it decreases rapidly afterwards to < 1.0 mg L^{-1} in 60 min in the AlZn50 alloy system (**Fig. 1d**). This indicates that Zn is the electron donor in AlZn20 and AlZn70 and both Al and Zn contribute to chemical reduction of Hg(Ⅱ) in AlZn50.

The declining concentration of Zn(Ⅱ) in the AlZn50 system (**Fig. 1d**) is the result of ZnAl-LDH precipitates, which are clearly detected by XRD characterization (**Fig. S1b**) in which the crystal planes of (003) and (006) match well with the typical planes of ZnAl-LDH [39, 40]. The ZnAl-LDH products are not identified in the AlZn20 and AlZn70 systems (**Fig. S1a, c**) due to low concentrations of Al^{3+} leached from these two alloys (**Fig. 1c**).

3.2 Effect of initial pH and capture capacity of Hg(Ⅱ) by AlZn alloys

Aqueous pH greatly affects metal speciation, surface charge of materials, redox potential of metals and many other surface characteristics [28, 41]. In general, the adsorption rate of heavy metals including Hg is greatly dependent on the pH of the solution [15]. For instance, Hg(II) is not removable in acidic pH ≤ 4 via adsorption, primarily because Hg^{2+} is poorly adsorbed by many absorbents (e.g. CTO-MFeS nanoparticles, polydopamine decorated SWCNTs) [42, 43]. By contrast, Hg(Ⅱ) is efficiently removed by ZVI via chemical reduction of Hg(Ⅱ) to Hg(0) in acidic waters but its removal rate is extremely poor in near neutral pH and above, due primarily to the surface passivation of ZVI particles and poor adsorption capacity of iron oxides on the surface [23, 24, 36]. In addition, Fe secondary contamination is a serious concern in the ZVI treatment system.

Fig. 2 shows the effect of initial pH 2-11 on Hg(Ⅱ) removal, pH variation during the removal process and leached Al(Ⅲ) and Zn(Ⅱ) concentration using AlZn50. Greater than 99.4% of 10 mg L^{-1} Hg^{2+} are removed in 3 min at initial pH values of 2-11. The pH of the solution increases to 5.9-8.2 from initial pH values of 2-7 while it decreases to 8.3-9.2 from initial pH values of 9-11 without using additional chemicals. These two features are particularly important for real-world applications. Leached concentrations of Al(Ⅲ) and Zn(Ⅱ) (**Fig. 2c, d**) indicate that Zn(0) is the major electron donor in acidic pH for Hg(Ⅱ) reduction while Al(0) contributes in neutral and alkaline pH values.

AlZn50 alloy removes 10-200 mg L^{-1} Hg(Ⅱ) rapidly and achieves removal efficiency of greater than 98% at pH 2 (**Fig. 3a**). The Hg(Ⅱ) removal process by AlZn50 follows a pseudo-second order of reaction at a rate constant of 0.0554 g mg^{-1} min^{-1} (**Figs. S3 and Tables S1**). The relatively low comparative error (χ = 0.0227) and high correlation coefficient (R^2=0.999) of the pseudo-second-order kinetic fitting demonstrate that the adsorption of Hg(II) on the surface of AlZn50 is dominated by chemical adsorption [44] while the Freundlich adsorption correlation coefficient (R^2=0.995) proves that the reaction is a multilayer adsorption process [45]. The measured and calculated capacities of Hg(Ⅱ) capture by AlZn50 at initial pH 2 is 4929 and 5155 mg g^{-1}, respectively (**Figs. S4 and Table S2**). Hg(II) capture capacity by traditional adsorbents ranges between 100-1000 mg g^{-1} at neutral and near neutral pH values [5, 15, 16, 23, 46-54] and the highest capacity is 4395 mg g^{-1} at pH 5.4-12 by thiol grafted imine-based covalent organic frameworks(TPB-DMTP-COF-SH) (**Table S3**). However, Hg adsorption capacity of COF composites is significantly reduced at pH 2, because the structure of COF collapses under acidic pH conditions and the positive charge of the COF surfaces repels Hg^{2+} ions [48, 55].

3.3 Reuse of AlZn alloys

Fig. 4 shows the removal efficiency of Hg(Ⅱ) in five cycles of AlZn50 alloy reaction with fresh Hg(Ⅱ) solutions. The removal efficiency reaches 98% in 3 min for each cycle. In each cycle of removal process, AlZn alloy was collected by centrifuge and filtration, washed with deionized water and dried at 60°C without any other re-generation steps. In this context, AlZn50 alloy for Hg(Ⅱ) removal is superior to many

adsorption materials. For instance, AgNPs covalent organic skeleton (AgNPs@COF) maintained a removal efficiency of 98% for 10 mg L^{-1} Hg after 5 cycles of repeated use in which the thermal decomposition and desorption were required to regenerate in each cycle [56].

3.4 Hg(Ⅱ) removal by AlFe alloys

The passivation is a critical factor affecting the performance/reactivity of zerovalent metals, bimetals and alloys for water remediation, due primarily to the formation of metal oxides and hydroxides, which are considered to improve adsorption of pollutants and on the other hand, to passivate the surface. In this context, AlFe alloys (10, 20 and 50% Fe) were also investigated along with zerovalent Fe and Al in this study (see **Supplemental Material Section I - Supplemental text Section I and Fig. S5-S11**). The findings of AlFe alloy investigations are (1) Hg(Ⅱ) removal rate increases with Fe concentration for 10 mg L^{-1} Hg(Ⅱ) at initial pH 2 and the highest rate of 99.6% is achieved by Fe(0), which simultaneously releases Fe ion concentration as high as 320 mg L^{-1}; (2) both Al(0) and Fe(0) in the AlFe alloys provide electrons for Hg(Ⅱ) reduction in acidic medium while Al(0) is the sole electron donor in alkaline pH medium; (3) the intermetallic compounds like Fe_4Al_{13} in AlFe alloys play an important role in catalyzing Hg(Ⅱ) reduction, improving the durability and reducing leached concentrations of Al and Fe ions.

3.5 Mechanism and capacity of Hg(Ⅱ) capture by AlZn and AlFe alloys

Previously, we observed that *in situ* formation of MgAl-LDH from MgAl alloys significantly improved the performance of MgAl alloys for removal of heavy metals and organic pollutants from water matrices [38]. Therefore, we consider that AlZn alloys remove aqueous Hg(Ⅱ) in a combined effect of chemical reduction, amalgamation, adsorption, surface complexation and co-precipitation associated with in-situ formation of ZnAl-LDH. We speculate that chemical reduction of Hg(Ⅱ) to Hg(0) is likely to dominate Hg(Ⅱ) removal and the amalgamation of Hg(0) with AlZn alloys might maintain the reactivity of AlZn alloys while *in situ* ZnAl-LDH's strong capabilities of adsorption and surface complexation may facilitate the removal process. The repeated use of AlZn50 alloy without performance deterioration (**Fig. 4**) may reveal that the generation of metal oxides, hydroxides and LDH on the surface of AlZn alloy does not have an adverse effect on Hg(Ⅱ) removal. Indeed, ZnAl-LDH is observed onto AlZn50 after treating Hg(Ⅱ) solution (**Fig. S1**). It is noted that no LDH products are identified in the cases of AlZn20 and AlZn70 and this is most likely because the concentration of Al^{3+} ions is not high enough (**Fig. 1c**) to induce the formation of LDH crystalline nucleation in this particular experiment. Nevertheless, ZnAl-LDH products are generated by increasing the dissolution rate of AlZn70 using pH 1 (HCl) solution with an extended reaction time (**Fig. 5**).

The initial pH affects the dissolution and hydrolysis rates of AlZn alloys (**Fig. 2**), the alloy's surface morphologies and the formation of hydroxides and ZnAl-LDHs (**Fig. S2**). To determine the contribution of ZnAl-LDH to Hg(Ⅱ) removal, we conducted the investigation in the following protocol. AlZn50 alloy was pretreated with pH 1 HCl solution for 72 h to coat a ZnAl-LDH film and then untreated alloy and pretreated alloy (p-AlZn50) were employed to treat 10 mg L^{-1} Hg(Ⅱ) solution at pH 1 and 12, respectively. During 72 h of the pretreatment, pH was lifted from 1 to 4.17 in 4 h and then slowly increased to 5.34 and remained unchanged, Al^{3+} concentration increased sharply to 2760 mg L^{-1} in 4 h, then slowly peaked to 3671 mg L^{-1} at 20 h and decreased rapidly to < 0.01 mg L^{-1} at 45 h (**Fig. S14**). By contrast, Zn^{2+} concentration increased rapidly to 2978 mg L^{-1} in 0.5 h and then declined to 1371 mg L^{-1} at 4 h. The decrease of Al^{3+} concentration is the result of ZnAl-LDH formation as confirmed by XRD, XPS, SEM and EDS characterization (**Fig. S15**). The diffraction peaks of p-AlZn50 at 11.7° and 23.6° correspond to the (003) and (006) planes in the ZnAl-LDH crystal phase [39, 40], which grows on the surface of AlZn50 alloy after pretreatment (**Fig. S15a**), changing the surface Al/Zn element ratio from 0.9:1 to 3:1 (**Fig. S15d, f**).

The concentration of Hg(Ⅱ), Zn(Ⅱ) and Al(Ⅲ) and pH profile during the reaction process of AlZn50 and p-AlZn50 with Hg(Ⅱ) solution at initial pH 1 and 12 are shown in **Fig. 6**. At both pH_0 = 1 and 12, AlZn50 removes Hg(Ⅱ) at >99% in 5 min (**Fig. 6 a, b**). In the case of pH_0 1, pH increases to 4.52 in 30 min and then remains unchanged in the following 120 min; Al^{3+} concentration increases to 395 mg L^{-1} in 60 min and then declines to 2.17 mg L^{-1} at 120 min while Zn^{2+} concentration increases to 584 mg L^{-1} in 30 min and then stays unchanged (**Fig. 6a**). In the case of pH_0 12, pH decreases rapidly to 9.56 in 5 min and Zn leaching is insignificant while Al^{3+} increases to 30 mg L^{-1} in 15 min and then remains constant (**Fig. 6b**). These observations demonstrate that both Al and Zn provide electrons for Hg(Ⅱ) reduction at pH_0 1 while Al(0) is likely the sole electron donor at pH_0 12.

The reaction of p-AlZn50 with aqueous Hg(Ⅱ) at pH_0 1 and 12 is different from that of AlZn50. Although no big differences in overall rates of Hg(Ⅱ) removal are observed between AlZn50 (**Fig. 6a**) and p-AlZn50

(**Fig. 6c**) at pH_0 1, Al^{3+} and Zn^{2+} concentration profiles differ to a large extent. Al^{3+} concentration increases monotonously to 990 mg L^{-1} in 120 min with p-AlZn50 while it peaks at 396 mg L^{-1} in 60 min with AlZn50. The leaching rate of Zn^{2+} is much slower with p-AlZn50 than that of AlZn50, but their final concentrations do not differ significantly (597 *versus* 591 mg L^{-1}). At pH_0 12, the overall rate of Hg(Ⅱ) removal by p-AlZn50 is the same as that by AlZn50 but the beginning rate is much slower (**Fig. 6b, d**). It is likely that Hg(Ⅱ) is removed by p-AlZn50 at pH_0 12 via ZnAl-LDH's isomorphous substitution and surface complexation rather than $Hg(OH)_2$ precipitation because Hg(Ⅱ) concentration is stable at pH 12 control (**Fig. 6b, d**).

AlZn50 and p-AlZn50 before and after Hg(Ⅱ) removal were characterized by XRD, SEM, XPS, FTIR and EDS (**Figs. 7, S16-19**). Elemental Hg is detected on the surface of AlZn50 at pH_0 1 while no Hg(0) is observed on the surface at pH_0 12 and LDH is identified in both cases (**Fig. 7a, b**). The characterization of AlZn50 and p-AlZn50 (**Figs. 7, S16-19**) indicates that chemical reduction is the primary path to capture Hg(Ⅱ) by AlZn50 under acidic pH conditions while Hg(Ⅱ) is removed by adsorption, coprecipitation and *i*LDH by AlZn50 at strong alkaline pH 12, as supported by the leaching concentration of Al^{3+} and Zn^{2+} (**Fig. 6a, b**). As for p-AlZn50, Hg(Ⅱ) is most likely removed by adsorption, coprecipitation and/or LDH's isomorphous substitution in both cases of pH_0 1 and 12. The variations in typical parameters of ZnAl-LDH before and after reaction of AlZn50 and p-AlZn50 with Hg(Ⅱ) (**Table S5**) probably reflect Hg(Ⅱ) incorporation into the ZnAl-LDH lattice via isomorphic substitution. It should be noted that chemical reduction could still contribute to aqueous Hg(Ⅱ) removal to a certain extent in the cases of AlZn50 at pH_0 12 and p-AlZn50 at pH_0 = 1.

Chemical reduction is also the major contribution to aqueous Hg(Ⅱ) removal by Fe(0), but the surface of Fe(0) is rapidly passivated by iron oxides and Fe(0) is not able to amalgamate with Hg(0) [9, 23]. Indium-doped Fe(0) improved Hg(Ⅱ) reduction by In-Hg amalgamation [9], but the improvement was not significant because the capture capacity was up to 300 mg g^{-1}. As for adsorption-dominated materials ([4, 43, 57] (e.g., COF-S-SH, Naf-LDH, $(SnS_4)^{4-}$/MgAl-LDH), Hg(Ⅱ) capture is governed by the surface charges of the adsorbents and aqueous pH, which determines mercury speciation (**Fig. S12**). Therefore, the competition between Hg^{2+} and H^+ ions explains that the majority of adsorption materials have poor adsorption at pH < 3 at which the speciation of Hg(Ⅱ) [15] is dominated by free Hg^{2+}. Both the positive and negative charges of adsorbents measured by Zeta-potential explained the adsorption of Hg(Ⅱ) at different pH values [43]. The pH_{PZC} (point of zero charge) of AlZn50 alloy is 8.6 (**Fig. S13**) and therefore, the rapid removal of Hg(Ⅱ) in a wide pH range of 2-11 indicates that adsorption does not dominate the process of Hg(Ⅱ) capture by AlZn50 alloy at acidic pH.

The theoretically estimated capacity of Hg(Ⅱ) capture by AlZn50 was 7000 mg g^{-1} if the electrons provided by Al and Zn were completely used for chemical reduction of Hg(Ⅱ). Therefore, further improvement from 4929 mg g^{-1} is possible by designing and manipulating the composition and surface structures of AlZn alloys to promote the effect of SRA-*i*LDH and to maximize the efficiency of electrons for Hg(Ⅱ) reduction. Al and Zn may be alloyed at any ratios without producing intermetallic compounds, thus creating the synergistic reductive amalgamation while the amphoteric properties of Al and Zn are conducive to capture Hg(Ⅱ) in a wide pH range from acidic to alkaline. Fe(0) is not able to amalgamate with Hg(0) while *in situ* generation of LDH was not observed in the treatment of acidic water by AlFe alloys [24, 58], due to rapid transformation of Fe^{2+} into $Fe(OH)_3$ precipitates at ambient and alkaline pH conditions [59-61]. In this context, AlZn alloys are superior to AlFe alloys for Hg-containing AMD treatment.

3.6 Acid mine drainage treatment

An AMD sample of pH 2.32 was treated using Al alloys (AlZn50, AlZn70, AlSi10, AlCu15 and AlFe50) and ZVI (**Table 1**). The Hg(Ⅱ) of 9.37 mg/L is removed in greater than 99% by all six materials while AlZn50 presents the best rate (99.8%) and ZVI gives the lowest rate (99.3%). The chemical reduction of Hg(II) to Hg(0) is considered to be the dominating factor. As for other heavy metals like Pb, As, Cu, Fe, Cd and Ni, AlZn50 also shows the best performance. Al^{3+} concentration is reduced to 0.001 mg/L from 673 mg/L by ZVI and it is likely due to the coprecipitation of $Al(OH)_3$ with $Fe(OH)_3$. Nevertheless, the dissolution of ZVI has resulted in a high Fe concentration of 2000 mg L^{-1}. Fe is one of the major contaminants in AMD. AlFe50 alloy removes Hg and other heavy metals in similar rates with ZVI, but does not remediate Al nor Fe contamination. Obviously, both AlFe alloy and ZVI are not suitable for AMD treatment. Similarly, AlSi and AlCu alloys do not remediate Al and Fe contamination of AMD. By contrast, AlZn50 and AlZn70 alloys show excellent performance of AMD treatment including Hg, other heavy metals, Al and Fe. However, releasing relatively high concentrations of Zn^{2+} is of concern and further Zn recovery is warranted. The reduction of Al^{3+} concentration in the cases of AlZn alloys is caused by the

formation of ZnAl-LDH (**Fig. S20).**

4. Conclusion

The removal of Hg(Ⅱ) from strongly acidic to alkaline aqueous solutions by AlZn alloys is simple, rapid and highly efficient. AlZn alloys are capable of capturing aqueous Hg(Ⅱ) at a capacity of 5000 mg g^{-1}, a record of the highest value reported so far. The super-performance of AlZn alloys for aqueous Hg(Ⅱ) capture is attributed to a synergistic effect of reductive amalgamation (SRA) of Hg with Al and Zn, reduction capability of Al and Zn at both acidic and alkaline conditions and *in situ* self-assemble of LDH (*i*LDH). The treatment of an acid mine drainage by different Al alloys and zerovalent iron (ZVI) deomonstrates that AlZn alloy presents the best performance of removing Hg, Fe, Al and many other heavy metals over AlFe, AlCu, AlSi alloys and ZVI. After treatment of AMD, further addressing weakly acidic pH values and relatively high concentrations of Zn ions is required and a simple neutralization could be suitable to rasie the pH values to neutral and near neutral and to recover Zn resources.

Data availability statement

All data generated and analyzed during this study are displayed in the article.

Supporting information

Supplementary data associated with this article can be found in the online version at Supplemental Material .docx.

References

[1] C.T. Driscoll, R.P. Mason, H.M. Chan, et al., Mercury as a global pollutant: sources, pathways, and effects, Environmental Science & Technology 2013;47:4967-4983.

[2] Q. Zhou, S. Wang, J. Liu, et al., Geological evolution of offshore pollution and its long-term potential impacts on marine ecosystems, Geoscience Frontiers 2022;13:

[3] Q. Wang, D. Kim, D.D. Dionysiou, et al., Sources and remediation for mercury contamination in aquatic systems-a literature review, Environmental Pollution 2004;131:323-336.

[4] N. Huang, L. Zhai, H. Xu, et al., Stable Covalent Organic Frameworks for Exceptional Mercury Removal from Aqueous Solutions, Journal of the American Chemical Society 2017;139:2428-2434.

[5] R. Fang, C. Lu, Y. Zhong, et al., Puffed rice carbon with coupled sulfur and metal iron for high-efficiency mercury removal in aqueous solution, Environmental Science & Technology 2020;54:2539-2547.

[6] X. Lu, X. Huangfu, J. Ma, Removal of trace mercury(II) from aqueous solution by in situ formed Mn-Fe (hydr)oxides, Journal of Hazardous Materials 2014;280:71-78.

[7] Q. Yu, J.B. Fein, Enhanced Removal of Dissolved Hg(II), Cd(II), and Au(III) from Water by Bacillus subtilis Bacterial Biomass Containing an Elevated Concentration of Sulfhydryl Sites, Environmental Science & Technology 2017;51:14360-14367.

[8] J.-H. Richard, H. Biester, Mercury removal from contaminated groundwater: Performance and limitations of amalgamation through brass shavings, Water Research 2016;99:272-280.

[9] G.H. Qasim, S. Lee, W. Lee, et al., Reduction and removal of aqueous Hg(II) using indium-modified zero-valent iron particles, Applied Catalysis B: Environmental 2020;277:

[10] X. He, X. Qiu, C. Hu, et al., Treatment of heavy metal ions in wastewater using layered double hydroxides: A review, Journal of Dispersion Science and Technology 2017;39:792-801.

[11] X. Feng, R. Long, L. Wang, et al., A review on heavy metal ions adsorption from water by layered double hydroxide and its composites, Separation and Purification Technology 2022;284:

[12] X. Yan, P. Li, X. Song, et al., Recent progress in the removal of mercury ions from water based MOFs materials, Coordination Chemistry Reviews 2021;443:

[13] S. Yu, H. Pang, S. Huang, et al., Recent advances in metal-organic framework membranes for water treatment: A review, Science of the Total Environment 2021;800:149662.

[14] X. Liu, H. Pang, X. Liu, et al., Orderly Porous Covalent Organic Frameworks-based Materials: Superior Adsorbents for Pollutants Removal from Aqueous Solutions, The Innovation 2021;2:100076.

[15] R. Soltani, R. Pelalak, M. Pishnamazi, et al., A water-stable functionalized NiCo-LDH/MOF nanocomposite: green synthesis, characterization, and its environmental application for heavy metals adsorption, Arabian Journal of Chemistry 2021;14:

[16] Y. Xiong, L. Su, H. Yang, et al., Fabrication of copper sulfide using a Cu-based metal organic framework for the colorimetric determination and the efficient removal of Hg^{2+} in aqueous solutions, New Journal of Chemistry 2015;39:9221-9227.

[17] K. Ai, C. Ruan, M. Shen, et al., MoS_2 Nanosheets with Widened Interlayer Spacing for High-Efficiency Removal of Mercury in Aquatic Systems, Advanced Functional Materials 2016;26:5542-5549.

[18] L. Merí-Bofí, S. Royuela, F. Zamora, et al., Thiol grafted imine-based covalent organic frameworks for water remediation through selective removal of Hg(II), Journal of Materials Chemistry A 2017;5:17973-17981.

[19] F. Fu, Z. Cheng, D.D. Dionysiou, et al., Fe/Al bimetallic particles for the fast and highly efficient removal of Cr(VI) over a wide pH range: Performance and mechanism, J Hazard Mater 2015;298:261-269.

[20] N. Singh, I. Srivastava, J. Dwivedi, et al., Ultrafast removal of ppb levels of Hg(II) and volatile Hg(0) using post modified metal organic framework, Chemosphere 2021;270:129490.

[21] A. Halder, S. Karak, M. Addicoat, et al., Ultrastable Imine-Based Covalent Organic Frameworks for Sulfuric Acid Recovery: An Effect of Interlayer Hydrogen Bonding, Angew. Chem. Int. Ed. 2018;57:5797-5802.

[22] K. Fu, X. Liu, C. Lv, et al., Superselective Hg(II) Removal from Water Using a Thiol-Laced MOF-Based Sponge Monolith: Performance and Mechanism, Environ Sci Technol 2022;56:2677-2688.

[23] T. Liu, Z.-L. Wang, X. Yan, et al., Removal of mercury (II) and chromium (VI) from wastewater using a new and effective composite: Pumice-supported nanoscale zero-valent iron, Chemical Engineering Journal 2014;245:34-40.

[24] J. Xu, Y. Pu, W.K. Qi, et al., Chemical removal of nitrate from water by aluminum-iron alloys, Chemosphere 2017;166:197-202.

[25] G.H. Qasim, S. Lee, G. Lee, et al., Dissolved oxygen and nitrate effects on the reduction and removal of divalent mercury by pumice supported nanoscale zero-valent iron, Environmental Science: Water Research & Technology 2018;4:1651-1661.

[26] W. Han, F. Fu, Z. Cheng, et al., Studies on the optimum conditions using acid-washed zero-valent iron/aluminum mixtures in permeable reactive barriers for the removal of different heavy metal ions from wastewater, Journal of Hazardous Materials 2016;302:437-446.

[27] Y. Zhang, S. Yang, Y. Zhang, et al., Enhancement of Cr(VI) removal by mechanically activated micron-scale zero-valent aluminum (MA-mZVAl): Performance and mechanism especially at near-neutral pH, Chemical Engineering Journal 2018;353:760-768.

[28] S. Yang, D. Zheng, T. Ren, et al., Zero-valent aluminum for reductive removal of aqueous pollutants over a wide pH range: Performance and mechanism especially at near-neutral pH, Water Research 2017;123:704-714.

[29] H.-L. Lien, W. Zhang, Enhanced dehalogenation of halogenated methanes by bimetallic CuAl, Chemosphere 2002;49:371-378.

[30] B. Yang, J. Zhang, Y. Zhang, et al., Promoting effect of EDTA on catalytic activity of highly stable Al–Ni bimetal alloy for dechlorination of 2-chlorophenol, Chemical Engineering Journal 2014;250:222-229.

[31] Z. Cheng, F. Fu, D.D. Dionysiou, et al., Adsorption, oxidation, and reduction behavior of arsenic in the removal of aqueous As(III) by mesoporous Fe/Al bimetallic particles, Water Res 2016;96:22-31.

[32] B. Yang, F. Zhang, S. Deng, et al., A facile method for the highly efficient hydrodechlorination of 2-chlorophenol using Al–Ni alloy in the presence of fluorine ion, Chemical Engineering Journal 2012;209:79-85.

[33] E. Kaprara, P. Seridou, V. Tsiamili, et al., Cu-Zn powders as potential Cr(VI) adsorbents for drinking water,

Journal of Hazardous Materials 2013;262:606-613.
[34] L. Zhang, X. Gao, Z. Zhang, et al., A Doping Lattice of Aluminum and Copper with Accelerated Electron Transfer Process and Enhanced Reductive Degradation Performance, Sci Rep 2016;6:31797.
[35] J. Xu, Y. Pu, X.J. Yang, et al., Rapid removal of chloroform, carbon tetrachloride and trichloroethylene in water by aluminum-iron alloy particles, Environ Technol 2018;39:2882-2890.
[36] J. Zhang, J. Wu, J. Chao, et al., Simultaneous removal of nitrate, copper and hexavalent chromium from water by aluminum-iron alloy particles, J Contam Hydrol 2019;227:103541.
[37] M. Hegedüs, K. Gáborová, T. Weidlich, et al., Rapid hydrodehalogenation of chlorinated benzoic acids using mechano-thermally prepared Raney alloy with enhanced kinetics, Journal of Environmental Chemical Engineering 2021;9:
[38] J. Zhang, H. Hu, J. Chao, et al., Groundwater remediation using Magnesium-Aluminum alloys and in situ layered doubled hydroxides, Environmental Research 2022;204:112241.
[39] G. Morales-Mendoza, F. Tzompantzi, C. García-Mendoza, et al., Mn-doped Zn/Al layered double hydroxides as photocatalysts for the 4-chlorophenol photodegradation, Applied Clay Science 2015;118:38-47.
[40] L. Cocheci, L. Lupa, R. Lazău, et al., Zinc recovery from waste zinc ash - A new “green” route for the preparation of Zn-Al layered double hydroxide used for molybdate retention, Journal of Alloys and Compounds 2019;787:332-343.
[41] B. Jiang, S. Xin, L. Gao, et al., Dramatically enhanced aerobic Cr(VI) reduction with scrap zero-valent aluminum induced by oxalate, Chemical Engineering Journal 2017;308:588-596.
[42] M. Sun, G. Cheng, X. Ge, et al., Aqueous Hg(II) immobilization by chitosan stabilized magnetic iron sulfide nanoparticles, Sci Total Environ 2018;621:1074-1083.
[43] S.S. Ghasemi, M. Hadavifar, B. Maleki, et al., Adsorption of mercury ions from synthetic aqueous solution using polydopamine decorated SWCNTs, Journal of Water Process Engineering 2019;32:
[44] A.A. Oladipo, E.O. Ahaka, M. Gazi, High adsorptive potential of calcined magnetic biochar derived from banana peels for Cu(2+), Hg(2+), and Zn(2+) ions removal in single and ternary systems, Environmental Science and Pollution Research 2019;26:31887-31899.
[45] Z. Ahmad, B. Gao, A. Mosa, et al., Removal of Cu(II), Cd(II) and Pb(II) ions from aqueous solutions by biochars derived from potassium-rich biomass, Journal of Cleaner Production 2018;180:437-449.
[46] J.D. Vernon, J.C. Bonzongo, Volatilization and sorption of dissolved mercury by metallic iron of different particle sizes: implications for treatment of mercury contaminated water effluents, Journal of Hazardous Materials 2014;276:408-414.
[47] K. Ai, C. Ruan, M. Shen, et al., MoS_2 nanosheets with widened interlayer spacing for high-efficiency removal of mercury in aquatic systems, Advanced Functional Materials 2016;26:5542-5549.
[48] L. Merí-Bofí, S. Royuela, F. Zamora, et al., Thiol grafted imine-based covalent organic frameworks for water remediation through selective removal of Hg(Ⅱ), Journal of Materials Chemistry A 2017;5:17973-17981.
[49] Q. Sun, B. Aguila, J. Perman, et al., Postsynthetically modified covalent organic frameworks for efficient and effective mercury removal, Journal of the American Chemical Society 2017;139:2786-2793.
[50] Y. Sun, Z. Lou, J. Yu, et al., Immobilization of mercury (II) from aqueous solution using Al_2O_3-supported nanoscale FeS, Chemical Engineering Journal 2017;323:483-491.
[51] R. Li, Y. Zhang, H. Deng, et al., Removing tetracycline and Hg(II) with ball-milled magnetic nanobiochar and its potential on polluted irrigation water reclamation, Journal of Hazardous Materials 2020;384:121095.
[52] L. Wang, M. Wang, Z. Li, et al., Enhanced removal of trace mercury from surface water using a novel Mg2Al layered double hydroxide supported iron sulfide composite, Chemical Engineering Journal 2020;393:
[53] K. Fu, X. Liu, C. Lv, et al., Superselective Hg(II) Removal from Water Using a Thiol-Laced MOF-Based

Sponge Monolith: Performance and Mechanism, Environmental Science & Technology 2022;56:2677-2688.
[54] T. Tene, F. Arias Arias, M. Guevara, et al., Removal of mercury(II) from aqueous solution by partially reduced graphene oxide, Scientific Reports 2022;12:6326.
[55] D. Saha, S. Barakat, S.E. Van Bramer, et al., Noncompetitive and Competitive Adsorption of Heavy Metals in Sulfur-Functionalized Ordered Mesoporous Carbon, ACS Appl Mater Interfaces 2016;8:34132-34142.
[56] L. Wang, H. Xu, Y. Qiu, et al., Utilization of Ag nanoparticles anchored in covalent organic frameworks for mercury removal from acidic waste water, Journal of Hazardous Materials 2020;389:121824.
[57] M. Shamsayei, Y. Yamini, H. Asiabi, Evaluation of reusable organic-inorganic nafion/layered double hydroxide nanohybrids for highly efficient uptake of mercury ions from aqueous solution, Applied Clay Science 2018;162:534-542.
[58] S. Wu, K. Tang, J. Zhang, et al., Removal of 4-chlorophenol from polluted water by aluminum-iron alloys, Water Sci. Technol. 2019;80:1099-1106.
[59] R. Chitrakar, Y. Makita, A. Sonoda, et al., Fe-Al layered double hydroxides in bromate reduction: Synthesis and reactivity, Journal of Colloid and Interface Science 2011;354:798-803.
[60] Y. Zhong, Q. Yang, K. Luo, et al., Fe(II)-Al(III) layered double hydroxides prepared by ultrasound-assisted co-precipitation method for the reduction of bromate, Journal of Hazardous Materials 2013;250-251:345-353.
[61] S. Aisawa, H. Hirahara, H. Uchiyama, et al., Synthesis and Thermal Decomposition of Mn–Al Layered Double Hydroxides, Journal of Solid State Chemistry 2002;167:152-159.

Figures

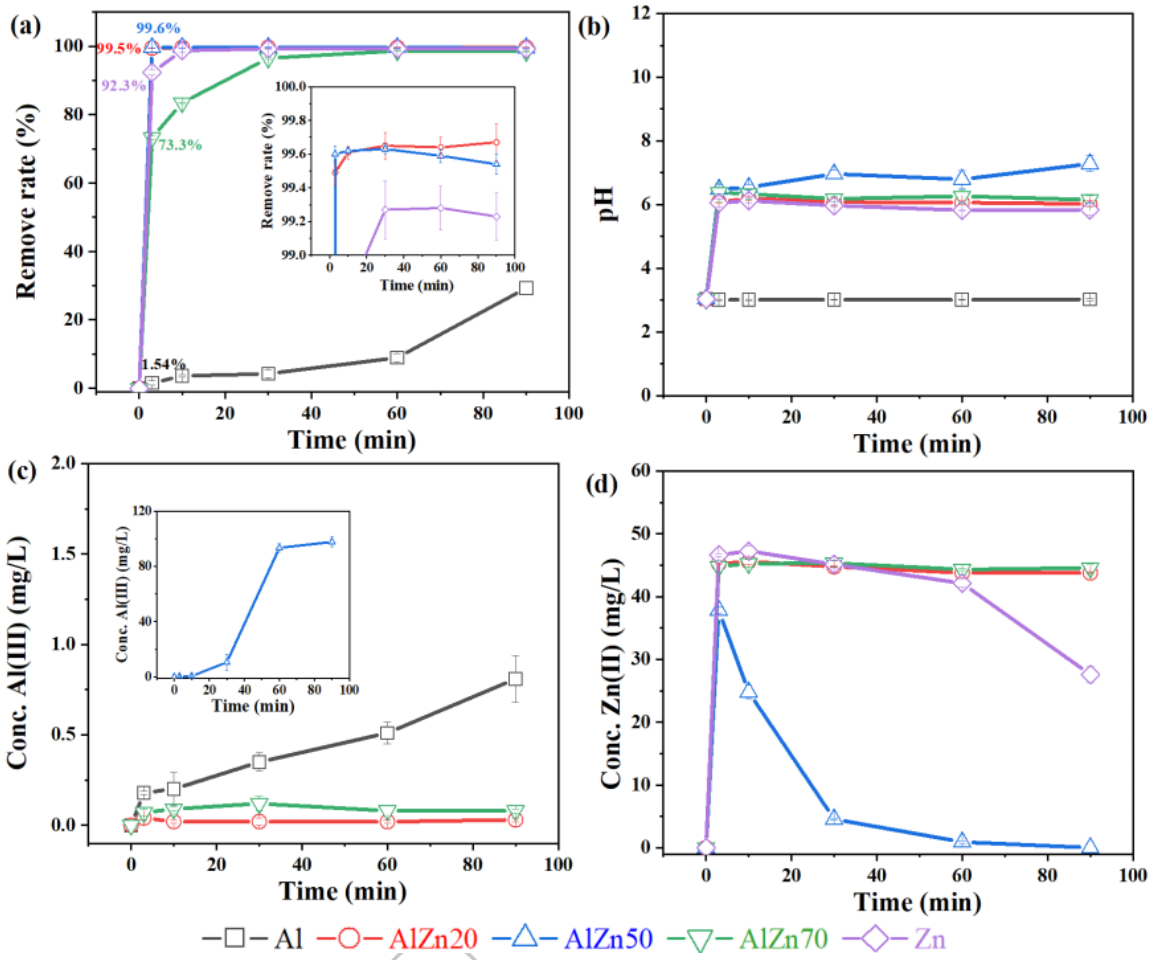

Fig. 1. Effect of Zn concentration in AlZn alloys on (a) Hg(Ⅱ) removal rate, (b) pH variation, (c) Al(Ⅲ) concentration, (d) Zn(Ⅱ) concentration. $[Hg(Ⅱ)]_0$=10 mg L^{-1}, V=45 mL, pH_0 = 3, material loading 0.5 g.

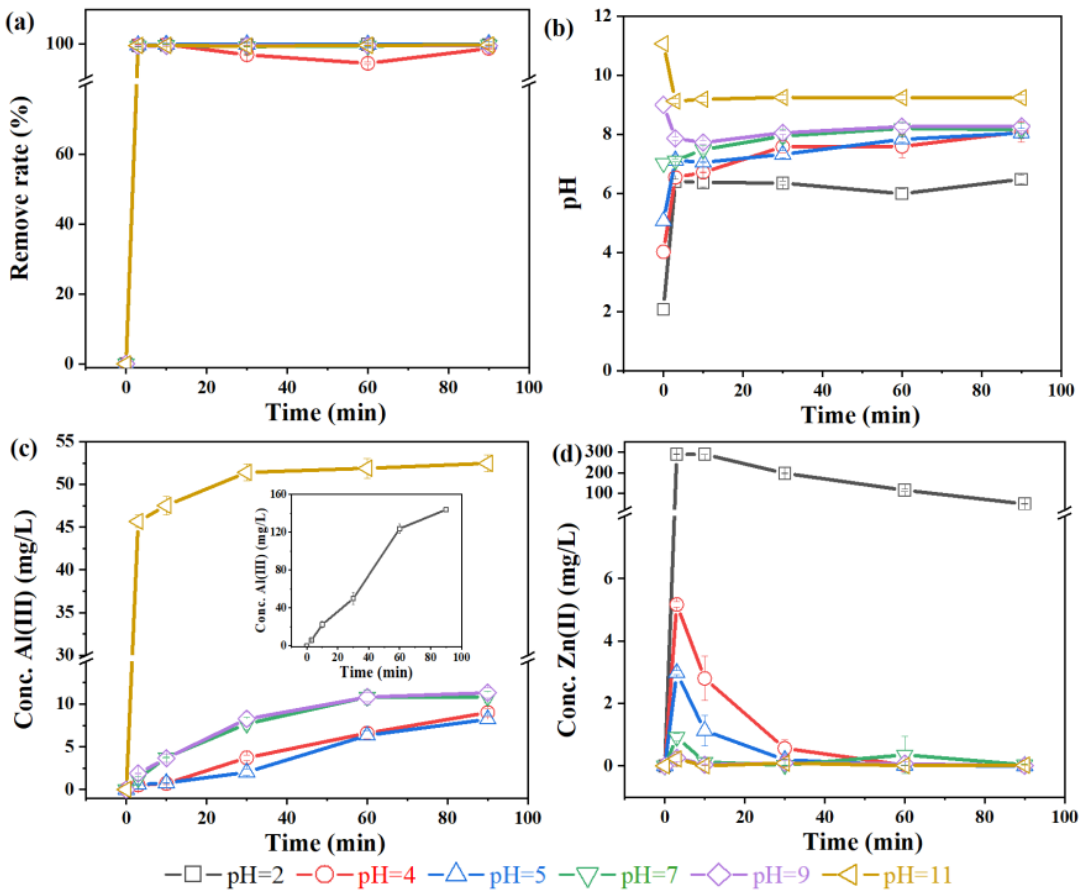

Fig. 2 Effect of initial pH on (a) Hg(Ⅱ) removal rate, (b) solution pH, (c) Al(Ⅲ) concentration, (d) Zn(Ⅱ) concentration. $[Hg(Ⅱ)]_0$=10 mg L^{-1}, V=45 mL, pH_0 = 2-11, AlZn50 alloy 0.5 g.

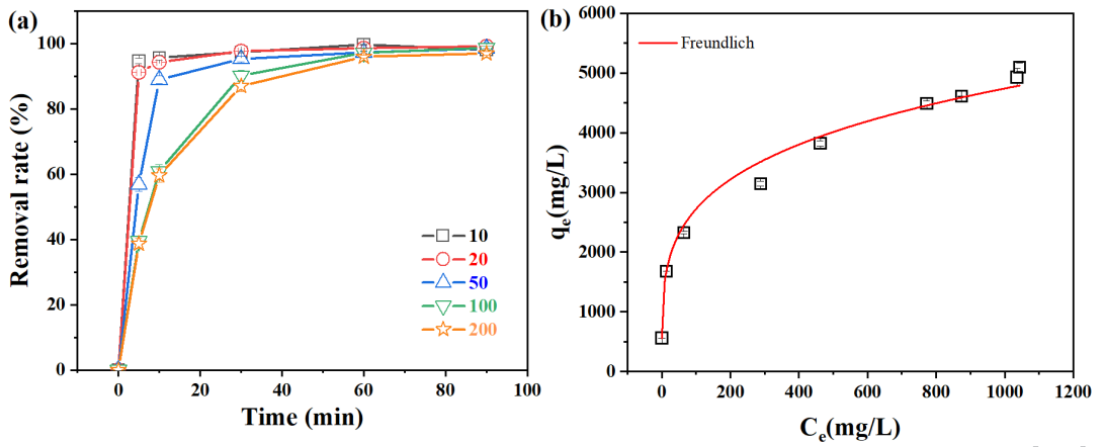

Fig. 3 (a) Effect of Hg(Ⅱ) concentration on removal rate as a function of rection time and (b) Hg(Ⅱ) removal capacity by AlZn50. $[Hg(Ⅱ)]_0$=10-2000 mg L^{-1}, V =45 mL, pH_0 = 2, AlZn50 alloy 0.01 g.

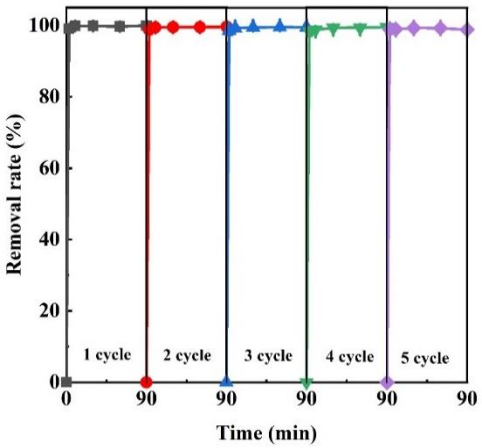

Fig. 4. Repeated use of AlZn50 alloy for removal of 500 mg L^{-1} Hg(Ⅱ). V=45 mL, pH_0 = 2, AlZn50 alloy 0.5 g.

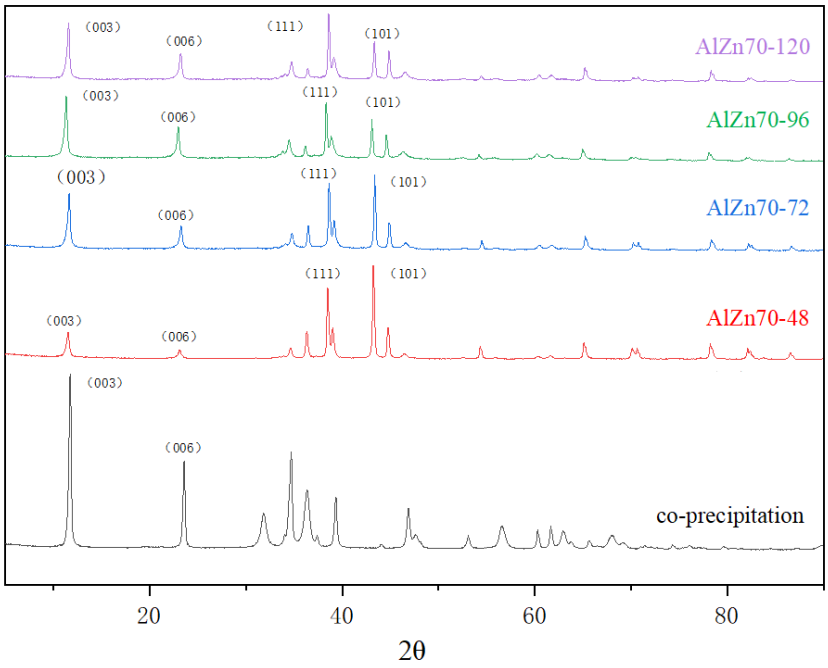

Fig. 5 XRD characterization of ZnAl-LDH by co-precipitation (CP) and AlZn70 alloy's hydrolysis at different time (48, 72, 96 and 120 h) and ambient temperature. 100 mL HCl, pH_0 = 1, AlZn70 alloy 1.5 g.

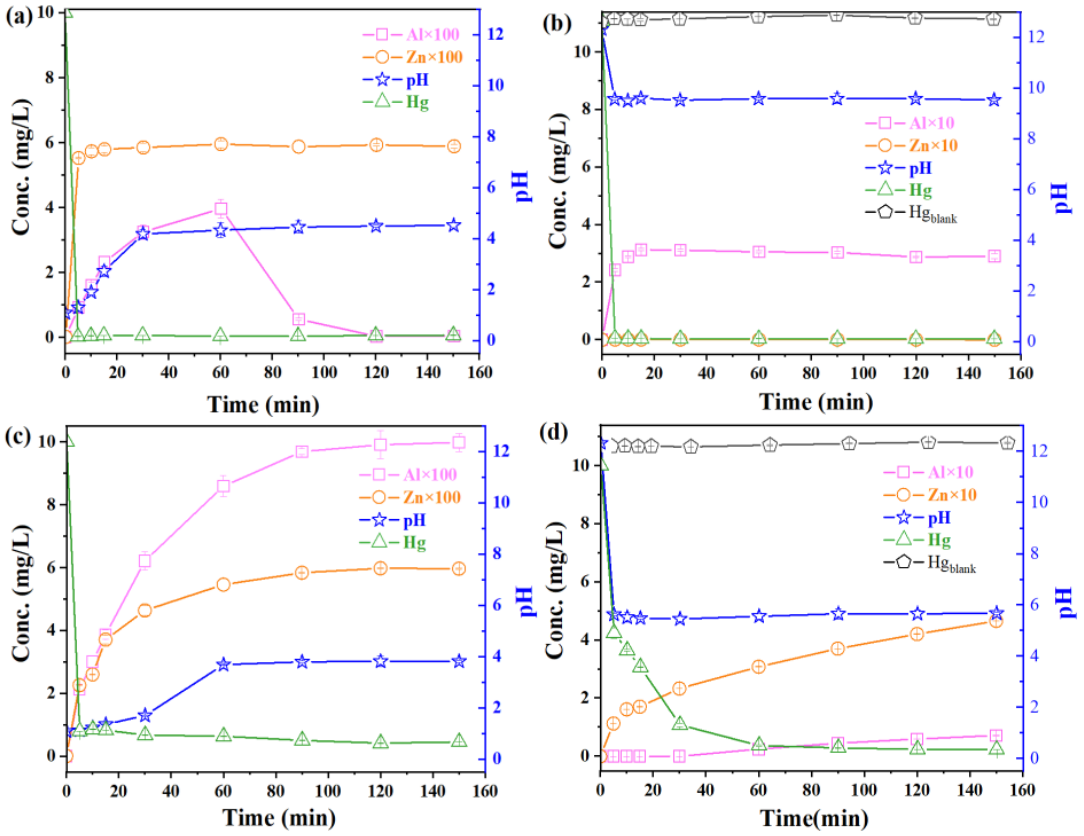

Fig. 6 Hg^{2+}, Al^{3+} and Zn^{2+} concentrations and pH changes during the reaction of AlZn50 and p-AlZn50 with Hg(Ⅱ) solution under different initial pH conditions (a) AlZn50 at pH 1, (b) AlZn50 at pH 12, (c) p-AlZn50 at pH 1, (d) p-AlZn50 at pH 12. $[Hg(Ⅱ)]_0$=10 mg L^{-1}, V=100 mL, pH_0 = 1 or 12, material loading

1.0 g.

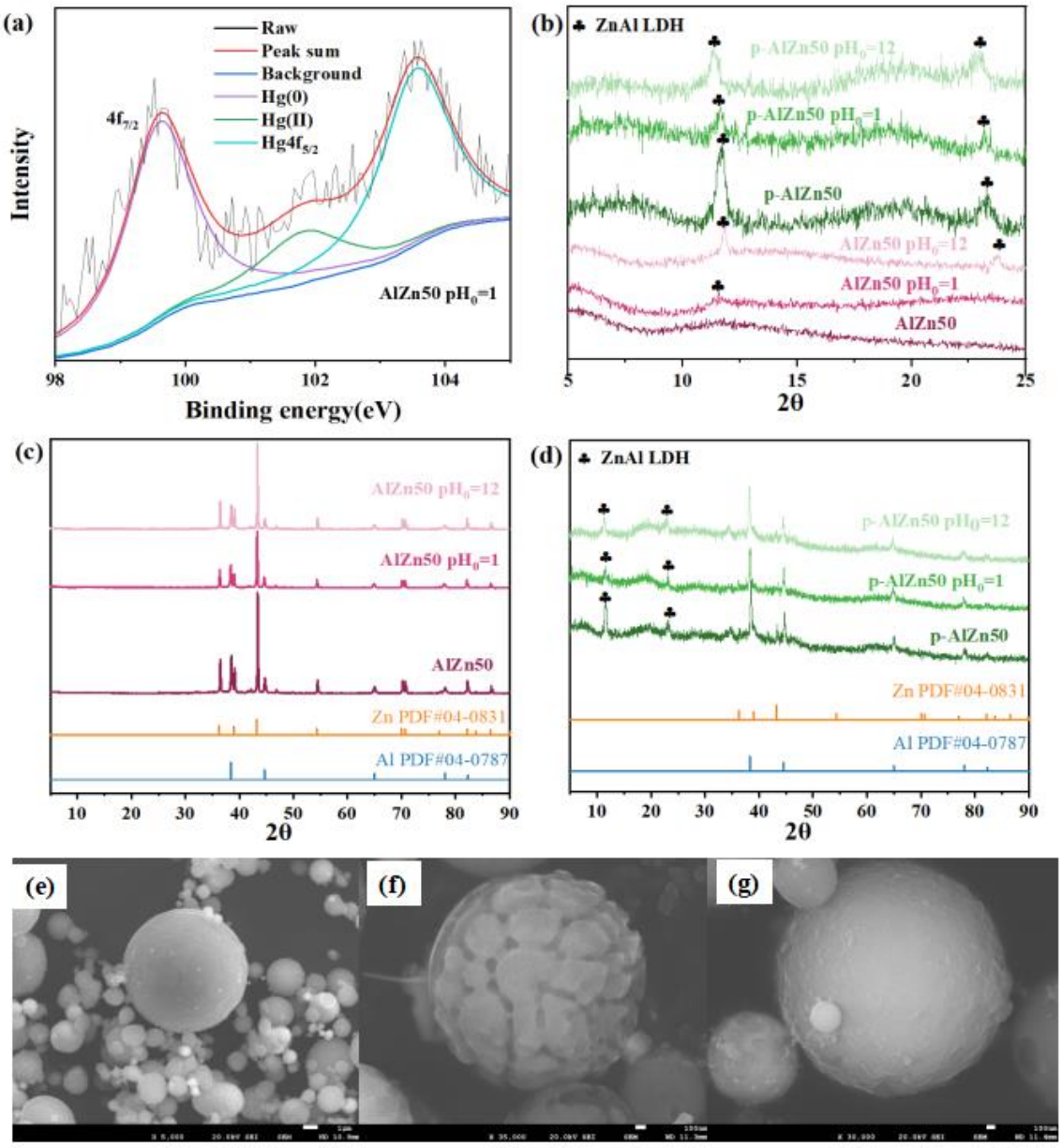

Fig. 7 XPS characterization of AlZn50 after reaction with Hg(Ⅱ) at pH 1 (a) Hg4f. XRD characterization before and after reaction of AlZn50 or p-AlZn50 (b) 2θ = 5-25°, (c) (d) 2θ = 5-90°. SEM characterization before and after reaction of AlZn50 (e) before the reaction, (f) after the reaction at pH 1, (g) after the reaction at pH 12. $[Hg(Ⅱ)]_0$=10 mg/L, V=100 mL, pH_0 = 1 or 12, material loading 1.0 g.

Table 1. Treatment of AMD by Al alloys and ZVI [a]

pH/ metals	Before treatment	After treatment					
		AlZn50	AlZn70	AlSi10	AlCu15	AlFe50	ZVI
pH	2.32	4.77	4.83	4.07	4.05	4.13	3.42
Hg	9.37	0.022	0.037	0.054	0.043	0.059	0.064
Al	673	/	/	716	481	470	/
Ca	444	445	440	441	440	443	440
K	5.11	5.12	5.13	5.01	5.14	5.09	5.07
Na	6.92	6.94	6.95	6.94	6.92	6.94	6.94
Pb	0.460	/	/	0.091	0.119	0.223	0.102
As	0.007	/	/	0.005	0.004	/	/
Ba	0.084	0.003	0.007	0.009	0.014	0.017	0.065
Cd	0.286	0.009	0.008	0.046	0.043	0.138	0.192
Cr	0.361	0.024	0.026	0.039	0.025	0.033	0.026
Cu	86.2	0.017	0.209	0.403	0.196	0.773	0.657
Fe	467	0.107	0.384	399	389	1139	2086
Mg	1564	1446	1451	1469	1503	1474	1498
Mn	118	118	118	118	118	117	118
Ni	4.74	0.097	1.64	4.00	3.92	4.19	0.093
Zn	6.14	1170	2263	6.13	6.15	/	6.14

[a] The AMD sample was collected from a copper mine site in Jiangxi Province, China. The concentration of each element is mg L^{-1} and $Hg(NO_3)_2$ solution was spiked to bring Hg(II) concentration to 10 mg L^{-1}. The dosage of material was 1 g 50 mL^{-1} in centrifuge tubes, agitated for 5 days at 45 rpm, temperature 25°C ± 2°C. The result is an average of three independent experiments. / indicates that the concentration is <0.001 mg L^{-1}.

Supplemental Material

Highly efficient capture of aqueous mercury by AlZn alloys via synergistic reductive amalgamation and in situ layered double hydroxide

Yetian Fang [a], Fangyuan Li [a], Jingbo Chao [b], Yang Tang [c], Frederic Coulon [d], Patrycja Krasucka [e], Patryk Oleszczuk [e], Qing Hu [f g], Xiao Jin Yang [a] *

[a] State Key Laboratory of Chemical Resource Engineering, Beijing University of Chemical Technology, Beijing 100029, China.

[b] National Institute of Metrology, Beijing 100029, China.

[c] National Fundamental Research Laboratory of New Hazardous Chemicals Assessment and Accident Analysis, Beijing University of Chemical Technology, Beijing, 100029, China

[d] School of Water, Energy and Environment, Cranfield University, Cranfield MK43 0AL, UK.

[e] Faculty of Chemistry, Department of Radiochemistry and Environmental Chemistry, Maria Curie-Sklodowska University, 3 M. Curie-Sklodowska Sq., 20-031 Lublin, Poland.

[f] Southern University of Science and Technology, Shenzhen, Guangdong 518055, China.

[g] Beijing Huanding Environmental Big Data Institute, No. 1 Wangzhuang Road, Beijing 100083, China.

*Corresponding Author: yangxj@mail.buct.edu.cn (X. J. Y.).

ORCID: Xiao Jin Yang: 0000-0003-4113-9298

Section I - Supplemental Text: Hg(II) removal by AlFe alloy

Effect of Fe content on Hg(Ⅱ) removal

Al, AlFe alloys (10, 20 and 50% Fe) are used to remove Hg(II) (**Fig S5**). The materials before and after Hg(II) removal were characterized by XRD and SEM (**Fig S6, S7**). The removal rate of Hg(Ⅱ) increased with the increase of iron content in the material. The removal rates of Hg(Ⅱ) reached 3.83%、67.26%、88.59%、90.86%、99.65% by Al, AlFe10, AlFe20, AlFe50 and Fe, respectively. **Fig. S5a** shows ZVI has the best removal efficiency, and the 80%removal rate is achieved in only 10 min of reaction. The lower removal rate of ZVAl is due to the protection of the surface oxide film. Its lower ion dissolution (0.58 mg L^{-1}, **Fig. S5 c**) also reflects its lower activity. **Fig. S5b** shows that the pH of the solution increases to 2.46, 2.87, 2.64, 2.42 and 4.75 from initial pH values of 2.3 by Al, AlFe10, AlFe20, AlFe50 and Fe, respectively. Nevertheless, the dissolved Fe concentrations in the AlFe10, AlFe20 and AlFe50 alloy were all lower than 20 mg L^{-1}. In contrast, the iron ion dissolution reached 305 mg L^{-1}. Although the AlFe alloy reduced the secondary pollution, the removal rate is still 8.79% lower than that of metal Fe in a short time.

Effect of initial pH on Hg(Ⅱ) removal by AlFe50 alloy

As the initial pH increased from 2 to 11, the removal rate of Hg(II) by AlFe50 decreased from 81.7% (pH_0=2) to less than 40% (pH_0=4), and then continued to increase to 90.6% (pH_0=11) (**Fig. S8a**). After reacting with Hg(II) the Al^{3+} concentration reached 6.22, 0.25, 0.063, 0.43, 1.93 and 11.1 by Al, AlFe10, AlFe20, AlFe50 and Fe, respectively (**Fig. S8c**). The change trend of Al^{3+} concentration with the increase of pH was consistent with the Hg(II) removal rate. However, the concentration of Fe ions (Fe(T)) gradually decreased. This shows that the role of Al in Hg(II) removal cannot be ignored and can be used to activate metal Fe. All in all, the change of pH had a great influence on the removal rate of Hg(Ⅱ). This point is obviously different from AlZn alloy, which may be related to the existence of alloy phase in AlFe alloy.

Removal results of different concentrations of Hg(Ⅱ) by AlFe50 alloy

With the increase of the initial Hg(Ⅱ) concentration, the removal of Hg(II) by AlFe50 increased. When the concentration of Hg(II) increased from 50 mg L^{-1} to 100 mg L^{-1}, the surface sites of AlFe50 were not saturated yet, so more Hg(II) could be bound. As the concentration continued to rise, the active sites of AlFe50 gradually saturated, resulting in the inability to remove a large amount of mercury ions, which greatly reduced the removal rate. Therefore, the removal capacity of Hg(Ⅱ) by AlFe50 reached 502.0 mg g^{-1} at C_0= 500 mg L^{-1}(**Table S4**). The limited adsorption capacity is related to the inability of Fe to form amalgam with Hg(0).

Reuse results of remove Hg(Ⅱ) by AlFe50 alloy

In order to evaluate the reuse effect of AlFe50 alloy, we reused it five times to study the removal rate of Hg(II) (**Fig. S11**). As the number of Hg(II) removal cycles increases, the removal rate of Hg(II) in the early

stage of the reaction decreased obviously and gradually, but the final removal rate was above 99% until the fourth cycle, and dropped to 97.9% in the fifth cycle. Due to the continuous corrosion and consumption of the alloy, the surface of the alloy is not all fresh active sites, and part of the area is covered by the generated (hydroxide) oxide, which reduces the electron transfer efficiency between the metal and Hg(II), and Hg(II) cannot be reduced immediately.

Section II – Supplemental Figures

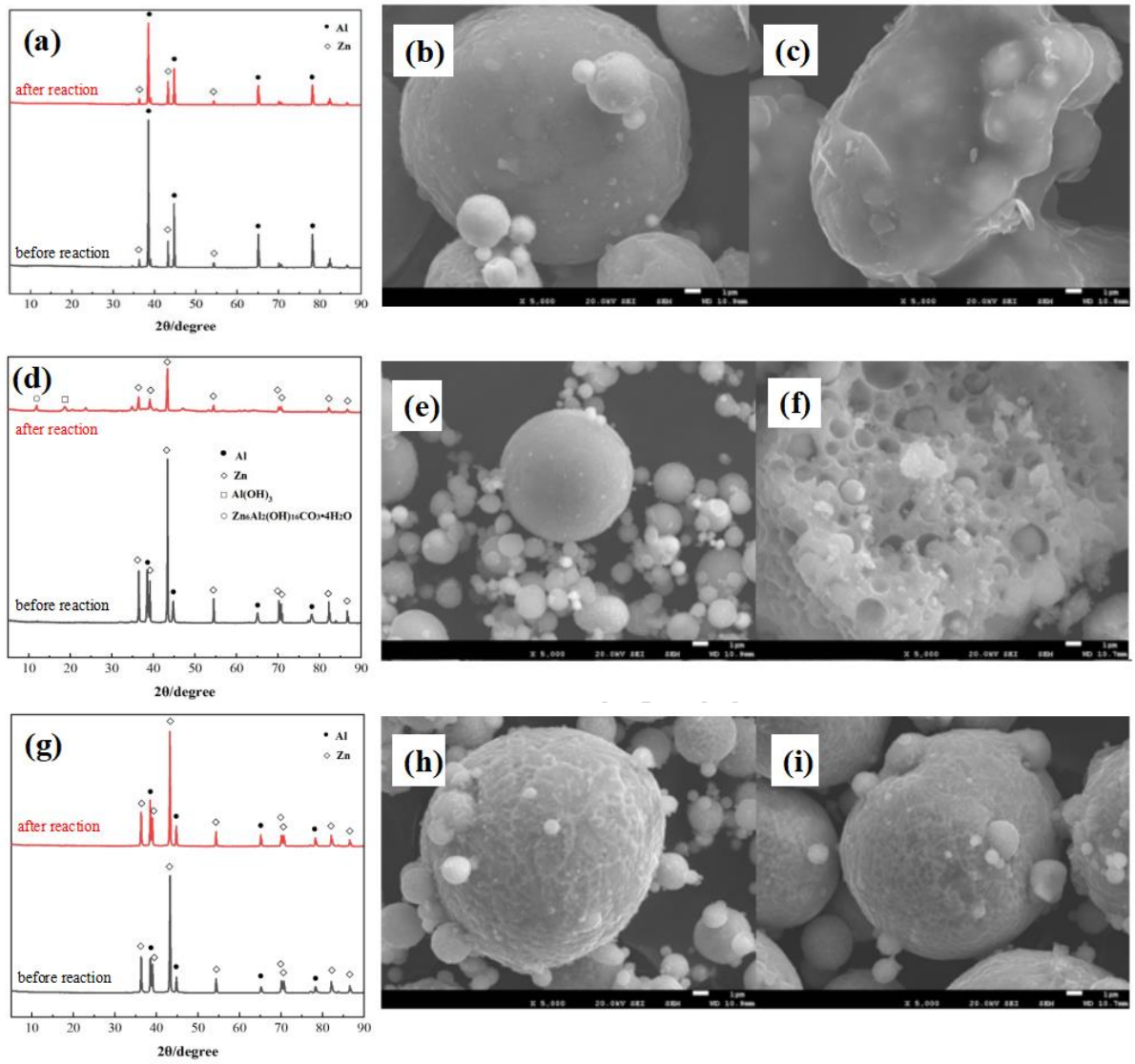

Fig. S1 XRD and SEM characterization of (a) - (c) AlZn20, (d) - (f) AlZn50 and (g) - (i) AlZn70. (b), I, (h) before the material reaction. (c), (f), (i) after the material reaction. $[Hg(II)]_0$=10 mg L^{-1}, V=45 mL, initial pH_0 = 3, material loading 0.5 g.

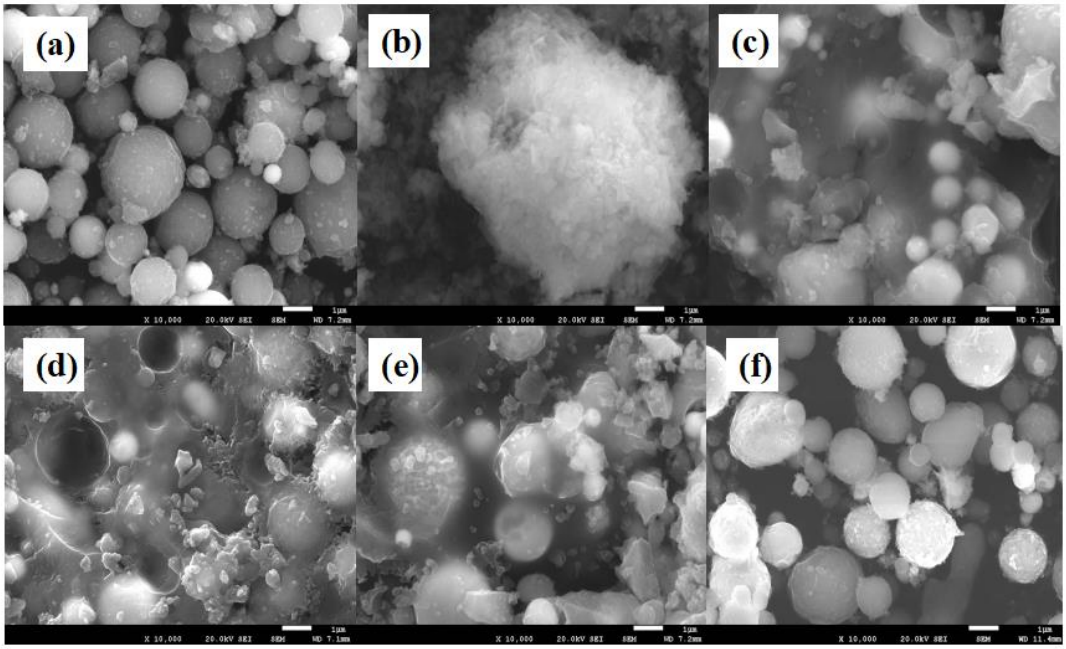

Fig. S2 SEM characterization of AlZn50 alloy after reaction under different pH conditions. (a) AlZn50 alloy before reaction, (b) initial pH 2, (c) initial pH 4, (d) initial pH 7, (e) initial pH 9, (f) initial pH 11. $[Hg(Ⅱ)]_0$=10 mg L^{-1}, V=45 mL, pH_0 = 2-11, AlZn50 alloy 0.5 g.

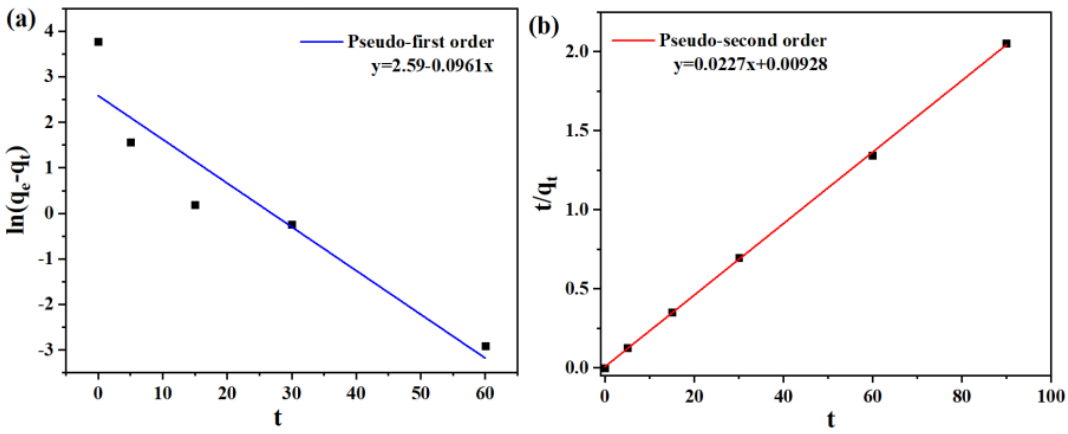

Fig. S3 Sorption kinetics (a) pseudo-first order, (b) pseudo-second order. $[Hg(Ⅱ)]_0$=10 mg L^{-1}, V=100mL, the initial pH was 2, AlZn50 alloy 0.01 g.

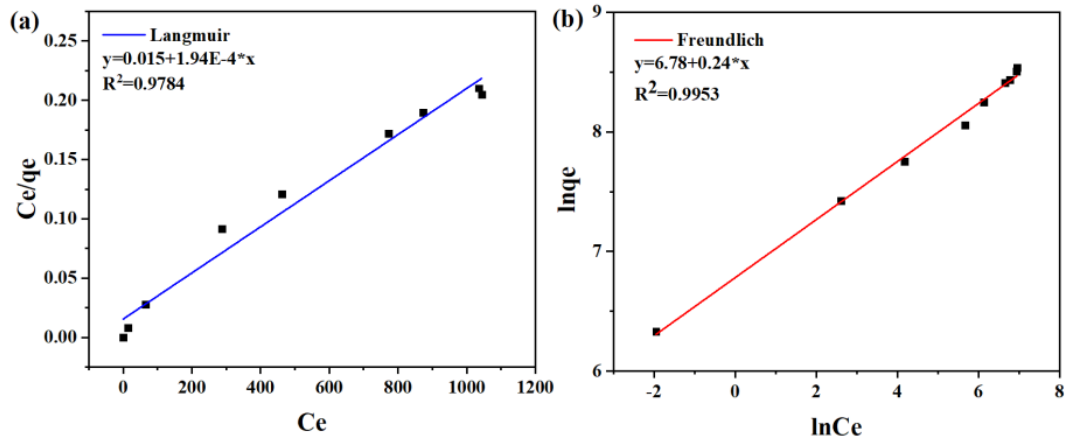

Fig. S4 Adsorption isotherm fitting (a) Langmuir, (b) Freundlich. $[Hg(Ⅱ)]_0$=10-2000 mg L^{-1}, V =100 mL, pH_0 = 2, AlZn50 alloy 0.01 g.

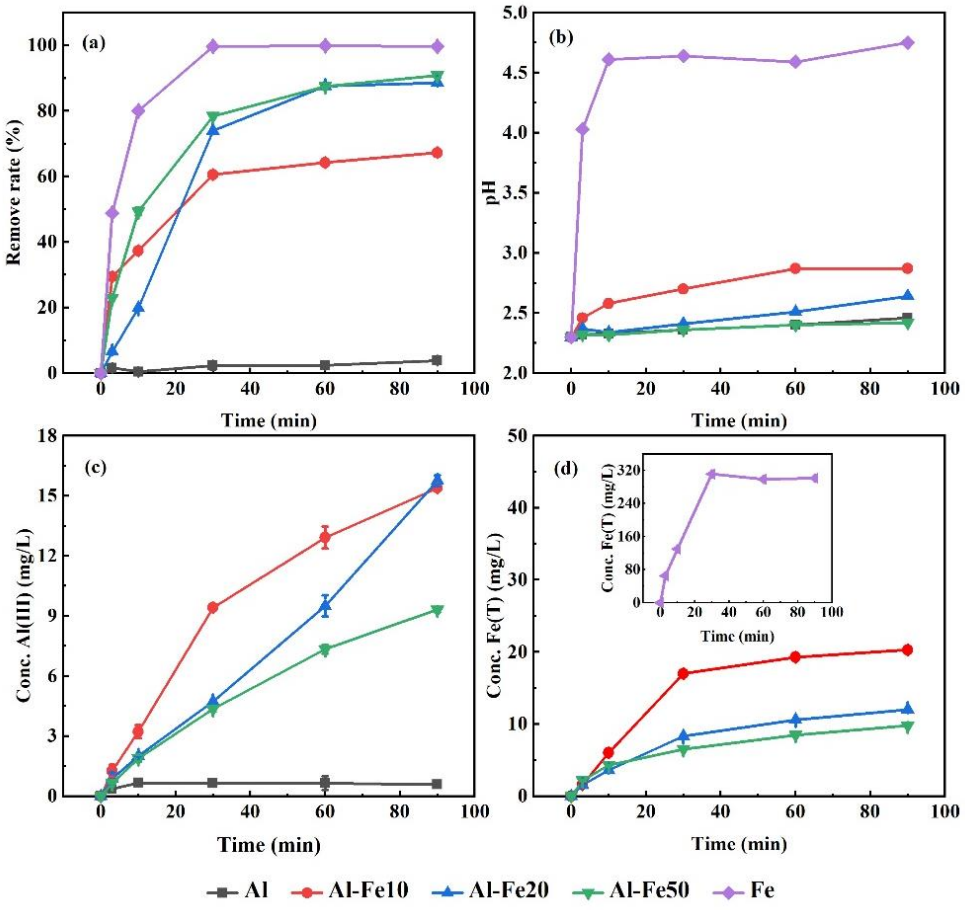

Fig. S5 Effect of Fe content on Hg(Ⅱ) removal. (a) removal rate, (b) solution pH variation, (c) Al(Ⅲ) concentration, (d) Fe(T) concentration. $[Hg(Ⅱ)]_0$=10 mg L^{-1}, V=45 mL, pH_0 = 2, material loading 0.5 g.

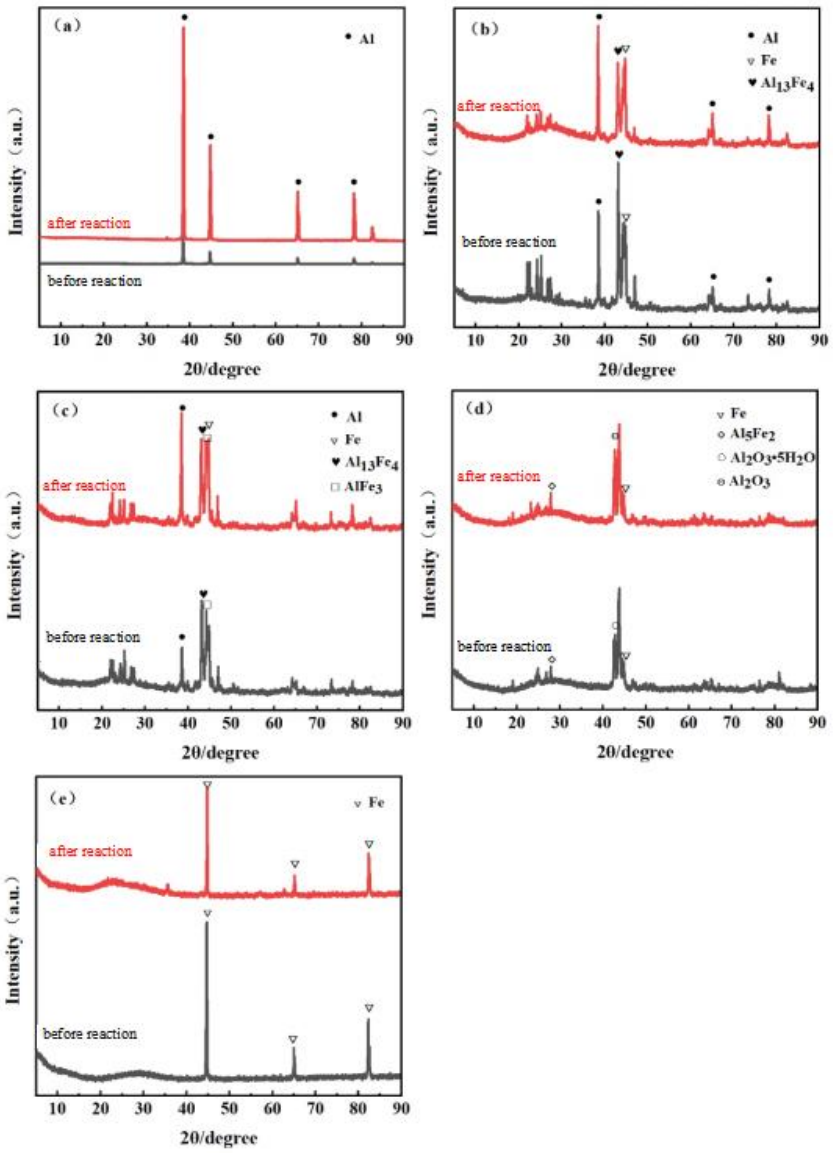

Fig. S6 XRD characterization of (a) Al, (b) AlFe10, (c) AlFe20, (d) AlFe50, and (e) Fe. $[Hg(Ⅱ)]_0$=10 mg L^{-1}, V=45 mL, pH_0 = 2, material loading 0.5 g.

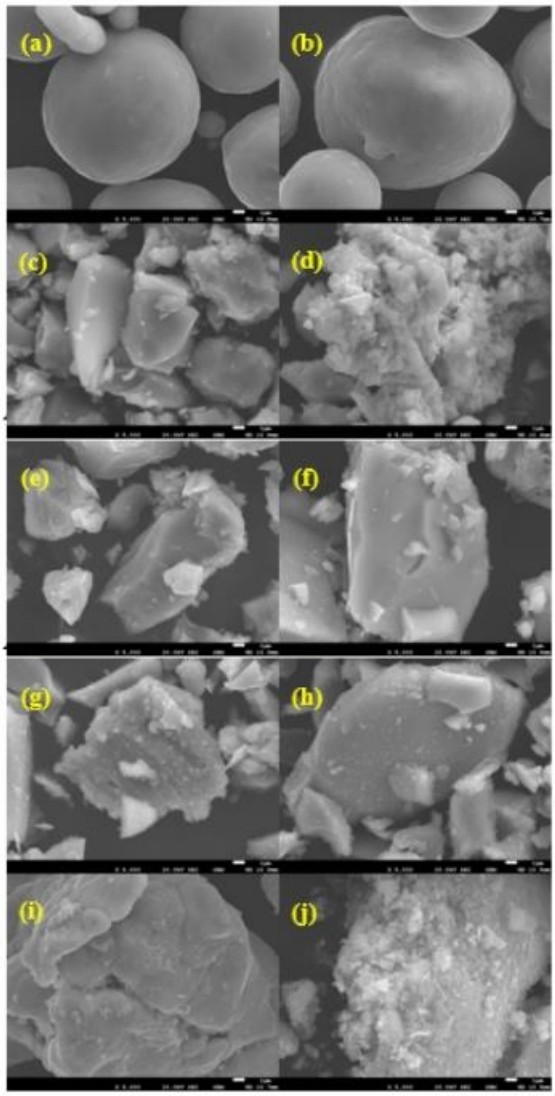

Fig. S7 SEM characterization of material before and after reacted with Hg(Ⅱ), (a) (b) Al, (c) (d)AlFe10, (e) (f) AlFe20, (g) (h) AlFe50, (i) (j) Fe. $[Hg(Ⅱ)]_0$=10 mg L^{-1}, V=45 mL, pH_0 = 2, material loading 0.5 g.

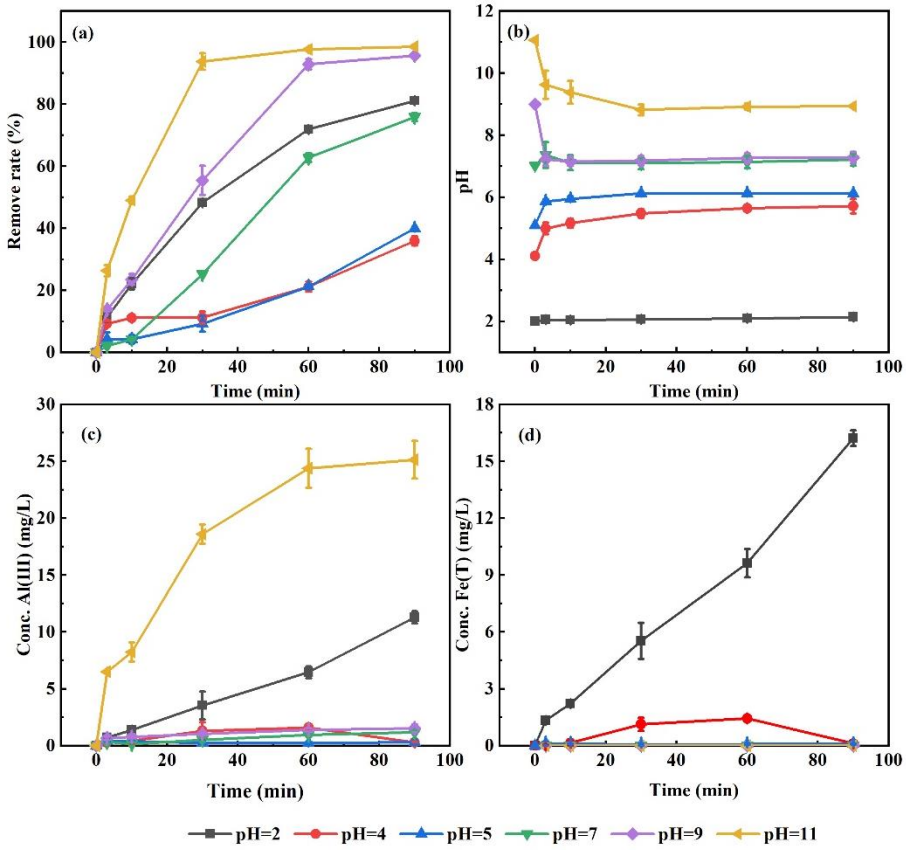

Fig. S8 Effect of initial pH on Hg(Ⅱ) removal by AlFe50 alloy. (a) removal rate, (b) solution pH, (c) Al(Ⅲ) concentration, (d) Fe(Total) concentration. $[Hg(Ⅱ)]_0$=10 mg L^{-1}, V=45 mL, pH_0 = 2, AlFe50 alloy 0.5 g.

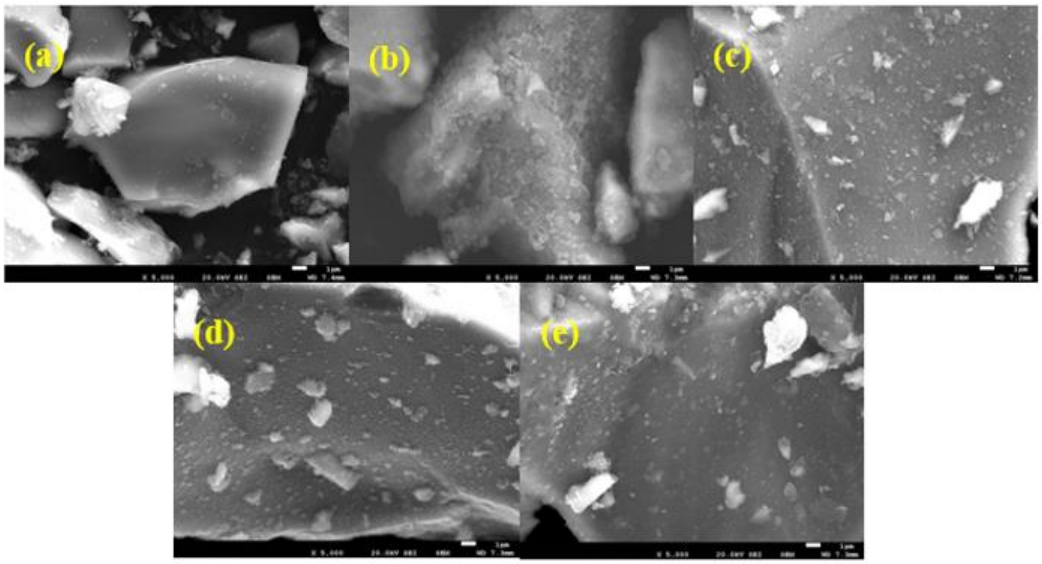

Fig. S9 SEM characterization of AlFe50 alloy after reaction under different pH conditions. (a) AlFe50 alloy before reaction, (b) initial pH 2, (c) initial pH 4, (d) initial pH 7, (e) initial pH 9. $[Hg(Ⅱ)]_0$=10 mg L^{-1}, V=45 mL, AlFe50 alloy 0.5 g.

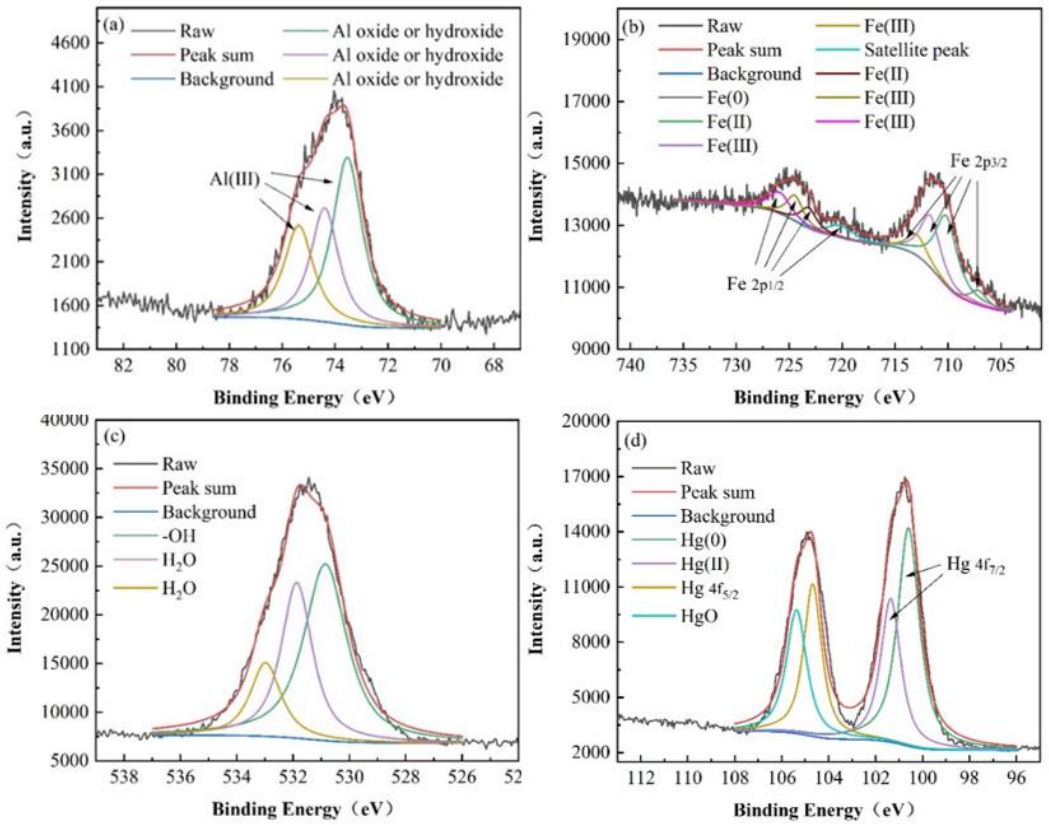

Fig. S10 XPS spectra of AlFe50 reacted with Hg(Ⅱ) (a) Al(2p), (b) Fe(2p) (c) O(1s), (d) Hg(4f). $[Hg(Ⅱ)]_0$=500 mg L^{-1}, V=45 mL, pH_0 = 2, AlFe50 alloy 0.5 g.

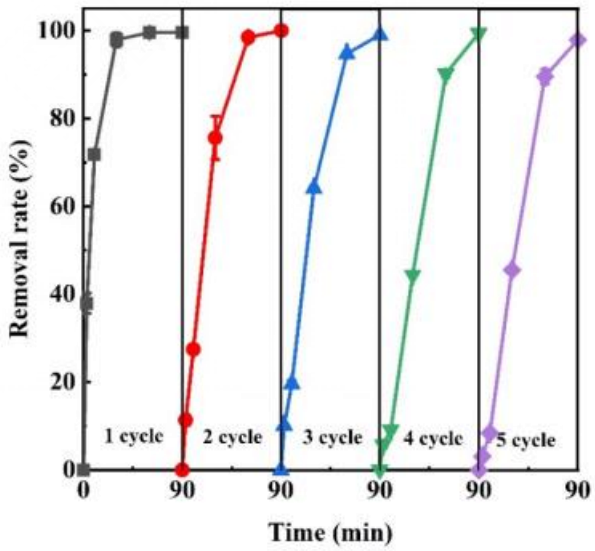

Fig. S11 Repeated use of AlFe50 alloy for removal of 500 mg L^{-1} Hg(II). V=45 mL, pH_0 = 2, AlFe50 alloy 0.5 g.

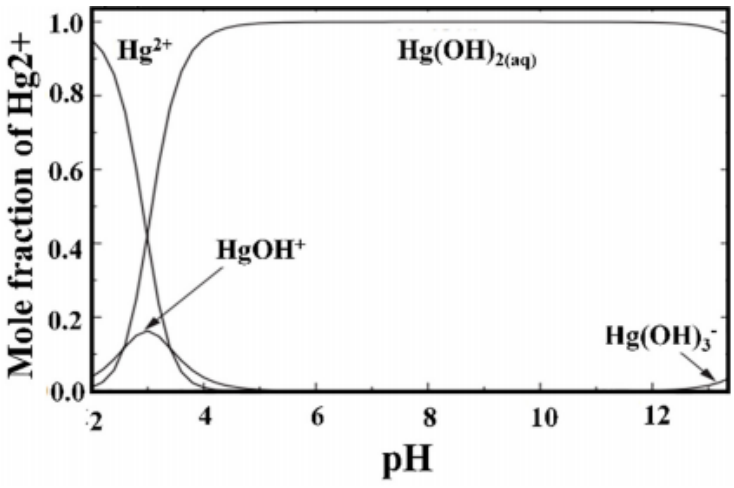

Fig. S12 Speciation diagram for Hg^{2+} ions.

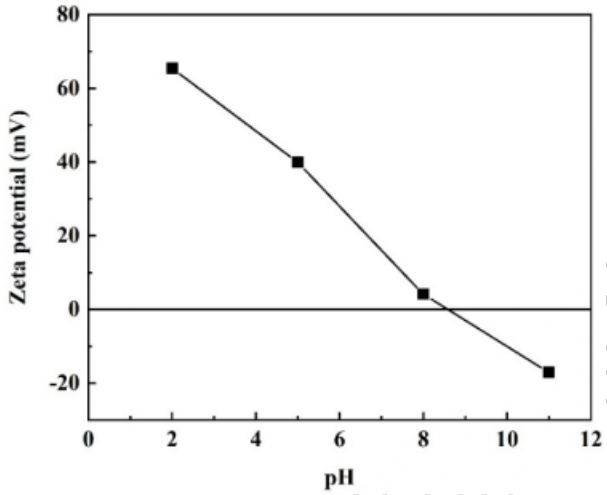

Fig. S13 Zeta Potential Diagram of AlZn50 Alloy.

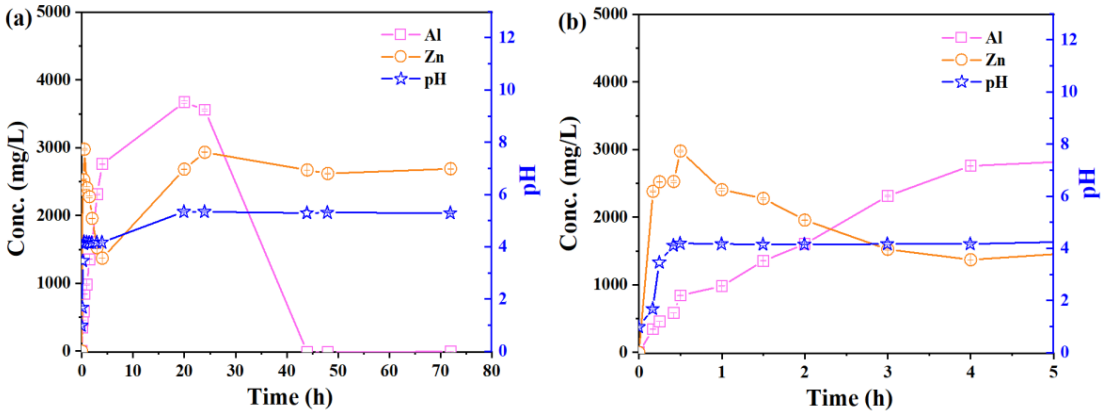

Fig. S14 Changes of ion dissolution concentration and pH of AlZn50 alloy during pretreatment (a) 0-72 h, (b) 0-5 h. V[HCl]=700 mL, pH_0 = 1, AlZn50 alloy 7 g.

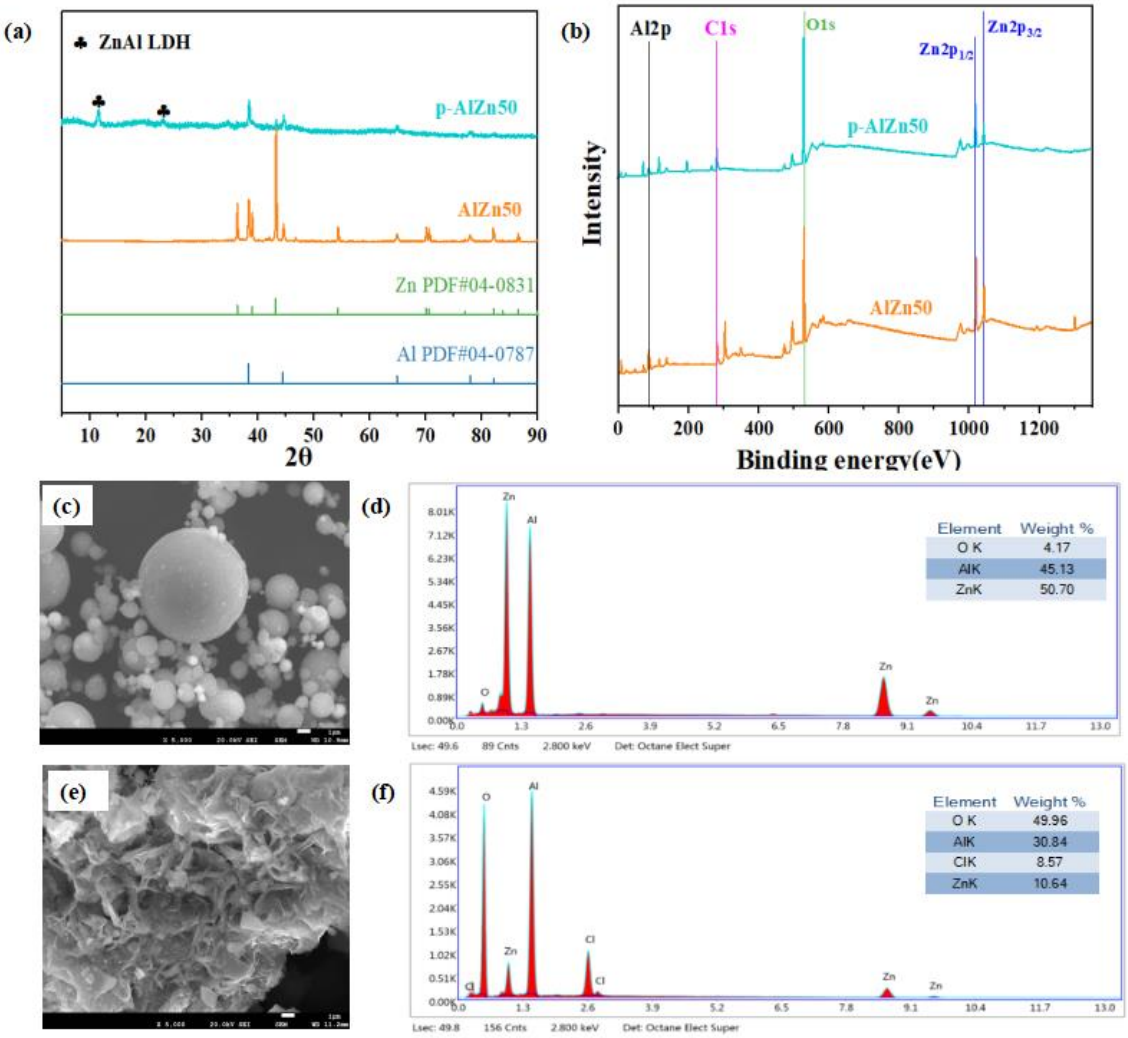

Fig. S15 (a) XRD characterization of AlZn50 and p-AlZn50, (b)XPS characterization of AlZn50 and p-AlZn50. SEM and EDS characterization (c) - (d) AlZn50, (e) - (f) p-AlZn50.

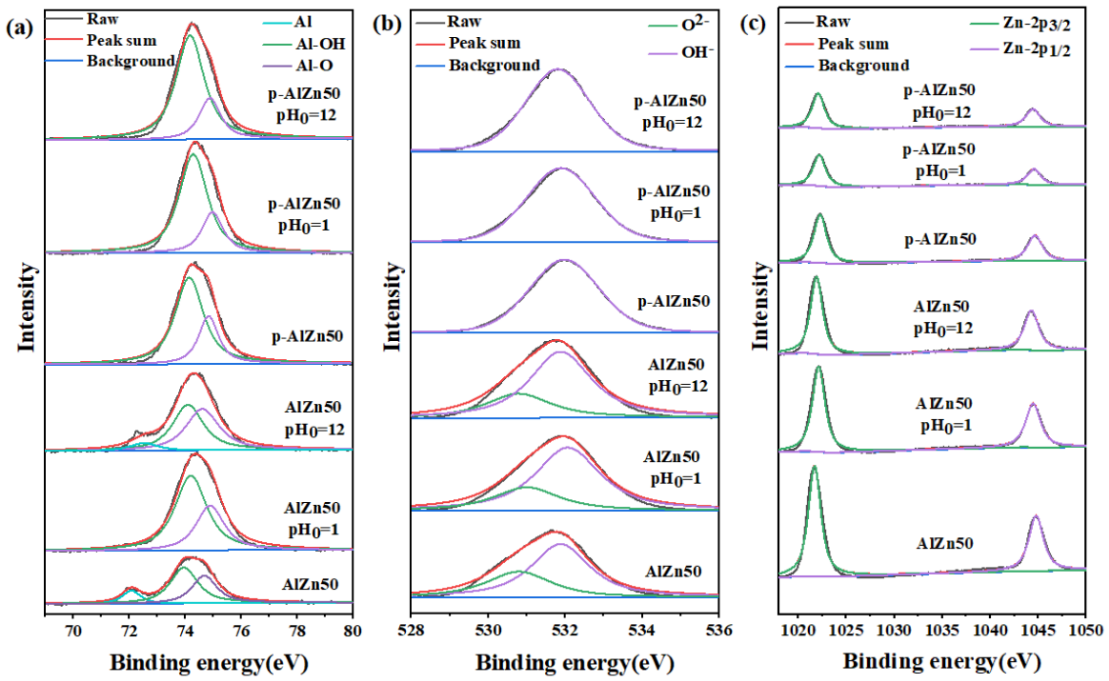

Fig. S16 XPS spectra of AlZn50 and p-AlZn50 materials reacted with Hg(Ⅱ) at pH 1 or 12 (a) Al(2p), (b) O(1s), (c) Zn(2p). $[Hg(Ⅱ)]_0$=10 mg L^{-1}, V=100 mL, pH_0 = 1 or 12, material loading 1.0 g.

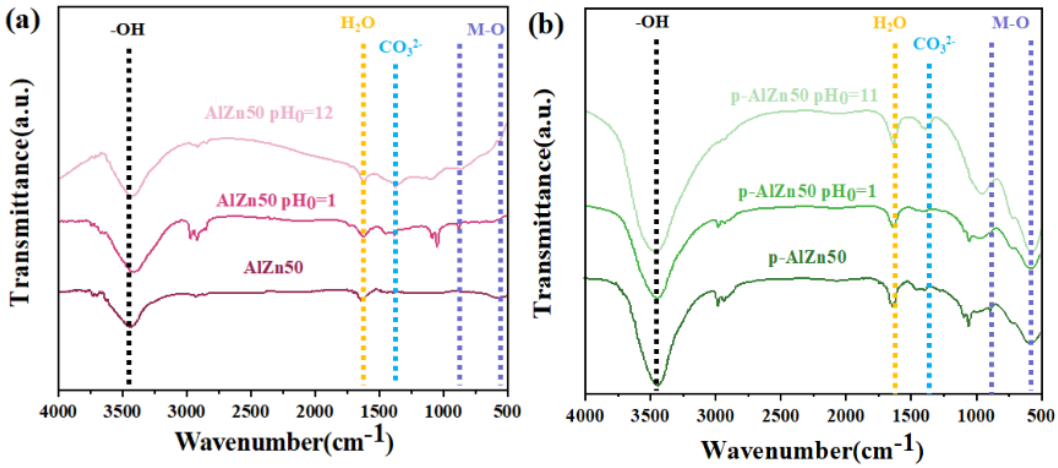

Fig. S17 FTIR characterization of AlZn50 and p-AlZn50 reacted with Hg(Ⅱ) at pH 1 or 12 (a) AlZn50, (b) p-AlZn50. $[Hg(Ⅱ)]_0$=10 mg L^{-1}, V=100 mL, pH_0 = 1 or 12, material loading 1.0 g.

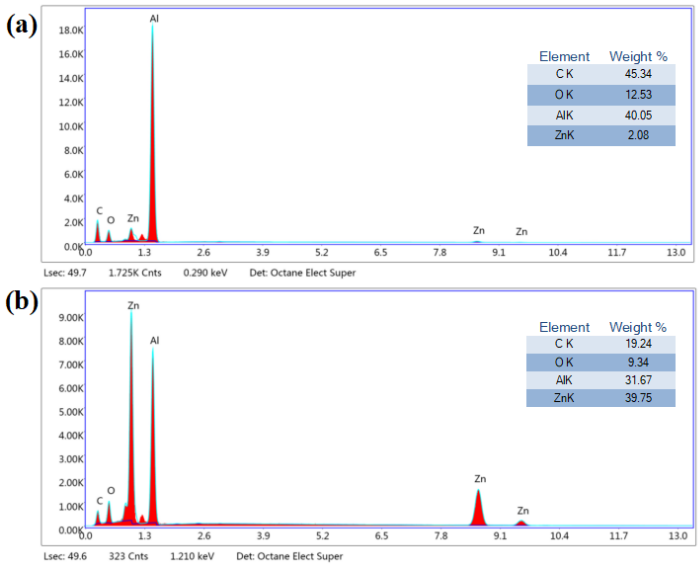

Fig. S18 EDS characterization of AlZn50 reacted with Hg(Ⅱ) at pH 1 or 12. (a) AlZn50 at pH 1, (b) AlZn50 at pH 12. $[Hg(Ⅱ)]_0$=10 mg L^{-1}, V=100 mL, pH_0 = 1 or 12, material loading 1.0 g.

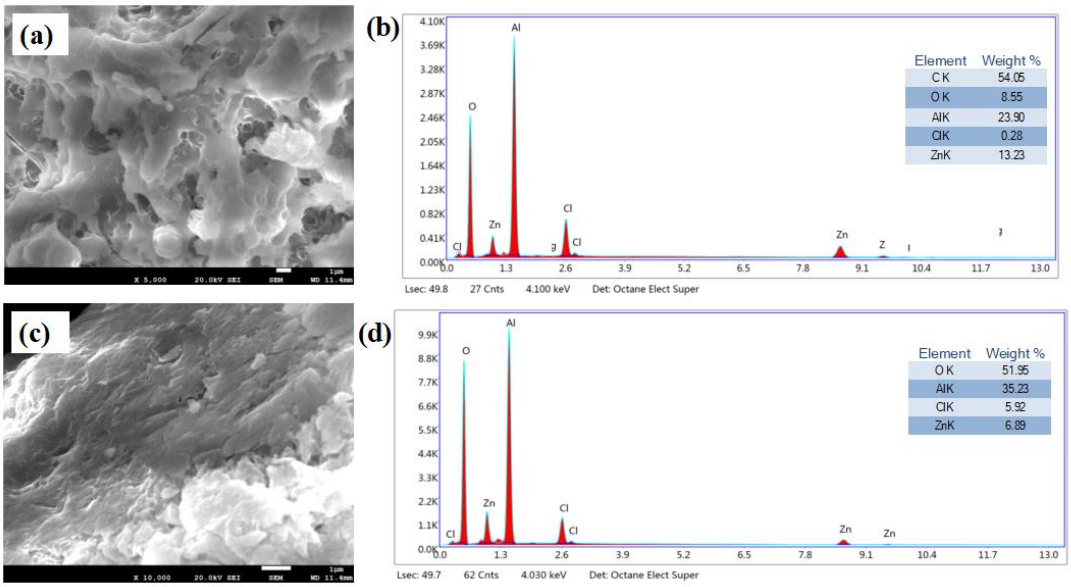

Fig. S19 SEM and EDS characterization of AlZn50 and p-AlZn50 reacted with Hg(Ⅱ) at pH 1 or 12 (a) - (b) p-AlZn50 at pH 1, (c) - (d) p-AlZn50 at pH 12. $[Hg(Ⅱ)]_0$=10 mg L^{-1}, V=100 mL, pH_0 = 1 or 12, material loading 1.0 g.

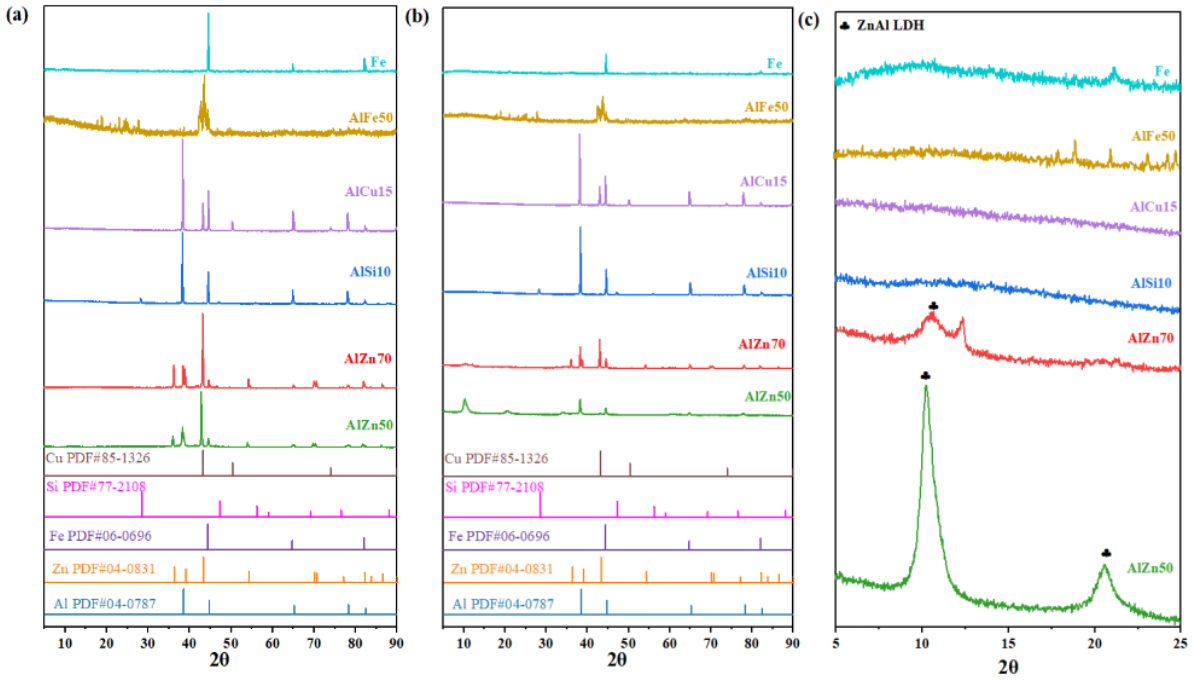

Fig. S20 XRD characterization of the reaction products of Al alloys and Fe. (a) before reaction, (b) after reaction 5-90°, (c) after reaction 5-25°. 80 mL AMD, pH_0 = 2.32, material loading 1.6 g, room temperature.

Section II – Supplemental Tables

Table S1 Adsorption kinetic fitting of Hg(II) adsorption by AlZn50 alloy. q_e (mg g^{-1}) is the adsorption capacity at equilibrium, q_t (mg g^{-1}) represents the adsorption amount at time t (min), k_1 is the pseudo-first-order model rate constant, and k_2 is the pseudo-second-order model rate. $[Hg(Ⅱ)]_0$=10 mg L^{-1}, V=100 mL, pH_0 = 2, AlZn50 alloy 0.01 g.

Model	Rate equation	Parameters	
Pseudo-first order	$\ln(q_e - q_t) = \ln q_e - k_1 t$	$q_{e,cal}$	13.3 mg g^{-1}
		k_1	0.0961 min^{-1}
		R^2	0.888
		$q_{e,exp}$	43.1 mg g^{-1}
		Δq_t	29.8
		□	2.24
Pseudo-second order	$\frac{t}{q_t} = \frac{1}{k_2 q_e^2} + \frac{1}{q_e} t$	$q_{e,cal}$	44.1mg g^{-1}
		k_2	0.0554 g mg^{-1} min^{-1}
		R^2	0.999
		$q_{e,exp}$	43.1 mg g^{-1}
		Δq_t	1.00
		□	0.0227

$\Delta q_t = | q_{e,exp} - q_{e,cal} |$, where $q_{e,exp}$ and $q_{e,cal}$ are the equilibrium experimental results and calculated value according the model, respectively. □ = Δq_t / $q_{e,cal}$.

Table S2 Adsorption isotherm parameters of Hg(II) adsorption by AlZn50 alloy. C_e (mg L^{-1}) is the Hg(Ⅱ) concentration at equilibrium, q_m (mg g^{-1}) is the adsorption capacity fitted by the model, K_L (L mg^{-1}), K_f (mg g^{-1}) are the Langmuir constant and Freundlich constant. $[Hg(Ⅱ)]_0$=200-2000 mg L^{-1}, V=100 mL, pH_0 = 2, AlZn50 alloy 0.01 g.

Sorption model	Linear equation	Parameters	
Langmuir	$\frac{C_e}{q_e} = \frac{1}{q_m K_L} + \frac{C_e}{q_m}$	q_m	5155 mg g^{-1}
		K_L	0.0129 L mg^{-1}
		R^2	0.978
		$q_{e,exp}$	4929 mg g^{-1}
		Δq_t	226
		□	0.0438
Freundlich	$\ln q_e = \frac{1}{n} \ln C_e + \ln K_f$	K_f	880 mg g^{-1}
		n	4.17
		R^2	0.995

Table S3 Comparison of adsorption capacity of AlZn50 alloy with other sorbents

Sorbents	Adsorption capacity ($mg\ g^{-1}$)	Ref.
rGO	110.21	[54]
FeS@Mg_2Al-LDH	116.96	[52]
Ball-milled magnetic nanobiochars (BMBCs)	127.4	[51]
FeS/Al_2O_3	313	[50]
p-nZVI	332.4	[23]
NiCo-LDH/MOF	509.8	[15]
PRC/Fe@S-10	738	[5]
nZVI	833	[46]
(MOF)-based sponge monolith (TLMSM)	954.7	[53]
COF-S-SH	1350	[49]
HKUST-1	2105	[16]
W-DR-N-MoS_2	2506	[47]
TPB-DMTP-COF-SH	4395	[48]
AlZn50 alloy	4929	This work

Table S4 Removal results of different concentrations of Hg(Ⅱ) by AlFe50.

$[Hg(Ⅱ)]_0$=50 - 500 mg L^{-1}, V=45 mL, pH_0 = 2, AlFe50 alloy 0.05 g.

C_0 ($mg\ L^{-1}$)	pH_0	final pH	ions concentration ($mg\ L^{-1}$)		q_e ($mg\ g^{-1}$)
			Al	Fe	Hg(Ⅱ)
50	2.04	2.05	3.37	3.17	139.6
100	2.07	2.10	3.29	3.35	255.4
300	2.07	2.15	2.26	2.28	373.9
500	2.00	2.07	0.21	0.14	502.0

Table S5 Crystallite size (*D*) of AlZn50 and p-AlZn50 materials before and after reacted with Hg(Ⅱ). $[Hg(Ⅱ)]_0$=10 mg/L, V=100 mL, pH_0 = 1 or 12, material loading 1.0 g.

$$D = \frac{K\lambda}{FWHM \cdot \cos\theta}$$

L is crystallite size, *K* is Scherrer parameter by default is taken 0.89, λ is X-ray wavelength taken as 0.15, *FWHM* (Full Width at Half Maximum) of the materials, θ is the Bragg diffraction angle, d is crystal planes spacing.

crystal planes	XRD structure parameters	LDH_1[a]	LDH_2[b]	LDH_3[c]	LDH_4[d]	LDH_5[e]
(003)	*d*(003)/nm	7.51	7.58	7.73	7.82	7.32
	2θ	11.78	11.66	11.44	11.30	12.08
	FWHM (rad)	0.37	0.53	0.22	0.98	0.48
	crystallite size in the c direction(nm)	0.38	0.26	0.62	0.14	0.29
(006)	*d*(006)/nm	3.81	3.84	3.71	/	3.82
	2θ	23.32	23.16	23.20	/	23.90
	FWHM (rad)	0.39	0.50	0.29	/	0.37
	crystallite size in the a direction(nm)	0.36	0.28	0.49	/	0.38

[a] LDH_1 is the LDH of p-AlZn50 before reaction.

[b] LDH_2 is the LDH after the reaction of p-AlZn50 at pH 1.

[c] LDH_3 is the LDH after the reaction of p-AlZn50 at pH 12.

[d] LDH_4 is the LDH after the reaction of AlZn50 at pH 1.

[e] LDH_5 is the LDH after the reaction of AlZn50 at pH 12.